LASER STABILIZATION EXPERIMENTS AND OPTICAL FREQUENCY COMB APPLICATIONS

by

Michael Kickbush

A Thesis

Submitted to the Faculty of Purdue University

In Partial Fulfillment of the Requirements for the degree of

Master of Science in Electrical and Computer Engineering

School of Electrical and Computer Engineering

West Lafayette, Indiana

August 2022

THE PURDUE UNIVERSITY GRADUATE SCHOOL
STATEMENT OF COMMITTEE APPROVAL

Dr. Andrew M. Weiner, Chair

School of Electrical and Computer Engineering

Dr. Peter Bermel

School of Electrical and Computer Engineering

Dr. Alexander Kildishev

School of Electrical and Computer Engineering

Approved by:

Dr. Dimitrious Peroulis

TABLE OF CONTENTS

LIST OF TABLES

LIST OF FIGURES

ABBREVIATIONS

AWG	Arbitrary Waveform Generator
CW	Continuous Wave
EDFA	Erbium-Doped Fiber Amplifier
EOPM	Electro-Optic Phase Modulator
FPC	Fabry-Pérot Cavity
FSR	Free Spectral Range
GNSS	Global Navigation Satellite Systems
MLL	Mode Locked Laser
PDH	Pound-Drever-Hall
PZT	Piezo Electric Transducer
Q	Quality Factor
SSM	Single Sideband Modulator
VCO	Voltage Controlled Oscillator
VNA	Vector Network Analyzer

ABSTRACT

In this Thesis I report on my work done in replicating the Pound-Drever-Hall (PDH) laser stabilization technique as well as applications of PDH to microring resonators and generated Optical Frequency Combs (OFC). These works have been broken down into three sections. First, I replicated the PDH method with a continuous wave (CW) laser along with a Fabry-Pérot Cavity (FPC). Second, I applied the same technique to a 25 GHz Free Spectral Range (FSR) microring resonator fabricated in Silicon Nitride. Third, I applied the PDH technique to a high Quality Factor (Q) high Free Spectral Range (FSR) microring resonator in preparation to lock the repetition rate of two soliton combs beat together. The last experiment was for an application towards a compact optical clock system; such systems will have a wide impact on the infrastructure of our navigation and communication structures in use today.

1. INTRODUCTION

Stable references are a hallmark of optical applications in use today. High Quality factor (Q) optical devices are often required to push the limits of current capabilities. Current SI seconds are based on the radiation of the ground state transition of caesium-133, with inaccuracies on the order of nanoseconds per day. Even better clocks have been created in recent years using cold strontium atoms and optical lattice layers with inaccuracies on the order of picoseconds per day [1][2]. While these methods are groundbreaking, they require large and often immobile designs. Pushing timekeeping capabilities today while keeping a system small enough for distribution requires miniaturization.

The potential of silicon nitride based microring resonators has been evolving in recent decades[3]. These high-Q resonators can create and sustain soliton frequency combs with repetition rates in the microwave regime. If leveraged properly, high-accuracy and portable timekeeping systems may be implemented in the near future[4].

Creating the foundation of an optical clock using microrings requires a pump laser that is locked using the resonances of the cavities. One reliable and powerful technique of locking a laser to a cavity is the Pound-Drever-Hall (PDH) frequency stabilization method. This thesis explores the work I have done with both PDH laser frequency stabilization as well as its potential use in locking a pump laser to a microring that is generating an optical frequency comb (OFC). The motivation for this final setup is to establish a detectable, stable microwave signal that can be used in future optical clock applications.

1.1 Pound-Drever-Hall

Optical continuous wave (CW) sources are subject to fluctuations in their radiation. This is primarily due to two factors: environmental effects (temperature, vibrations, etc.) and random spontaneous emissions inside the laser cavity [5]. These factors can alter the frequency and linewidth of the CW source, which disrupt applications that require a stable frequency and predictable linewidth. The Pound-Drever-Hall (PDH) technique, first introduced in 1983 demonstrated the stabilization of a CW source by locking the source to an high Q optical cavity to control the linewidth of an output pump signal [6][7]. An example

of a PDH setup can be seen in Figure 1.1. In the case of microring resonators, this linewidth has been demonstrated to be further improved by offsetting the cavities with materials that offer a negative thermo-optic coefficient [8].

In the first two experiments of this thesis, this frequency control was accomplished by a servo controller connected to the Piezo-Electric Transducer (PZT) that controlled cavity of the CW laser. The first was performed with a high Finesse Fabry-Pérot Cavity (FPC), while the second and third was performed with microring resonators fabricated in silicon nitride.

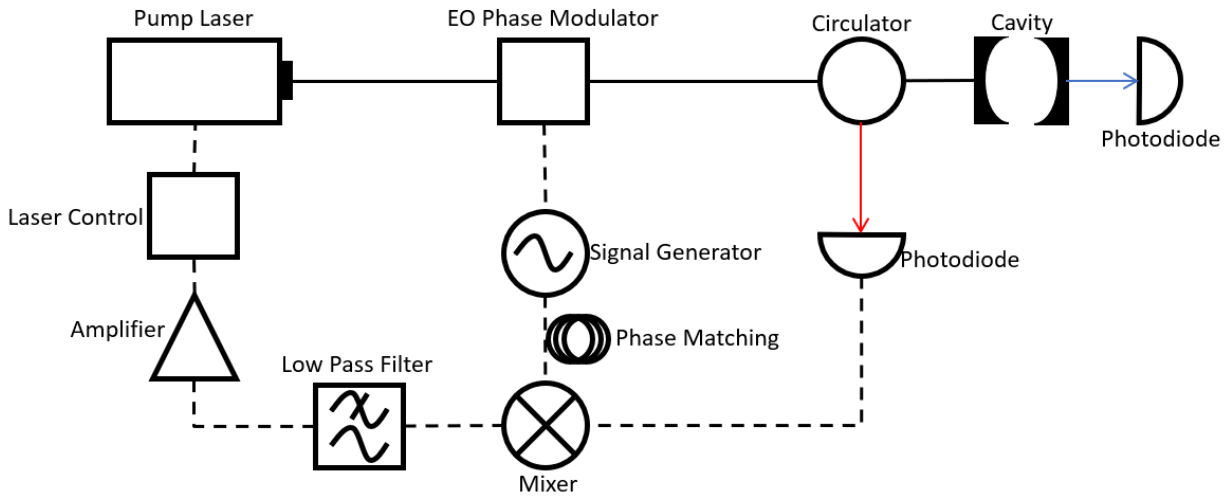

Figure 1.1. Example of a general Pound-Drever-Hall frequency stabilization setup

Typically, a PDH lock is accomplished with the use of a Fabry-Pérot Cavity (FPC), or Fabry-Pérot interferometer, which is an optical cavity made from two thin reflective surfaces introduced in 1899. [9] When optical light is in resonance with the cavity, it allows transmission of the resonant light. By operating a CW laser with tuning capabilities near resonance, we can feed the reflected signal back to some laser control and hold it at its minimum. This decouples the natural fluctuations in intensity and frequency made by the pump laser [10]. The difficulty is knowing which way to tune the laser when power reflected by the FPC is nonzero. In the frequency domain, this reflected intensity will be symmetric around the FPC resonance. However, this signal's derivative with respect to frequency will be anti-symmetric, and this can be used to distinguish which side of resonance the pump is at any given moment. This is accomplished by phase modulating the pump light prior to

contact with the cavity, and then mixing the reflected intensity with the same modulation signal to get a dc response that will be anti-symmetric around zero [10]. This signal is what is typically called the error signal, capable of being used by a control system. Examples of PDH error signals are shown in Figures 1.4 and 1.5.

A measure of the optical resonant response of a FPC is its Finesse. Finesse is a measure of this resonance response in relation to how far apart the resonances occur, also known as the Free Spectral Range (FSR) [11]. Mathematically, Finesse is the FSR divided by the full-width half-maximum of the resonant response.

$$F = \frac{FSR}{FWHM} \tag{1.1}$$

What this means is that the sharpness of a cavity's response is due to the internal losses. With light reflecting between the mirrors of the cavity, some will be lost every round trip through the mirrors, often defined by a reflection coefficient R_n. A higher reflectivity of the mirrors leads to higher Finesse of the cavity. This can be shown with a simulation of FPCs with differing Finesse values. Figures 1.2 and 1.3 show simulated transmission spectra with Finesse values at 50 and 150 respectively. The higher Finesse of Figure 1.3 shows a narrower response in the frequency domain on resonance. It should be noted that the mirrors of these simulated cavities are the same, that is $R_1 = R_2$.

Finesse is related to the Quality factor (Q) of a cavity, but only through the optical frequency that is being used. The relationship is:

$$Q = F \times \frac{\nu_{resonance}}{FSR} \tag{1.2}$$

[11]

Where the resonant frequency in the cavity determines the Q. This equation is just another form of the bandwidth definition for Q, where $Q = \frac{\nu_0}{\Delta\nu_{FWHM}}$.

However, without a method of phase matching, the amplitude of the error signal may not be ideal. To understand this, a look at the phase relation of the transmitted and reflected beams of the FPC is necessary. In a cavity with two mirrors, when the pump is perfectly at the resonance of the FPC, the light reflected from the first mirror and the second mirror will

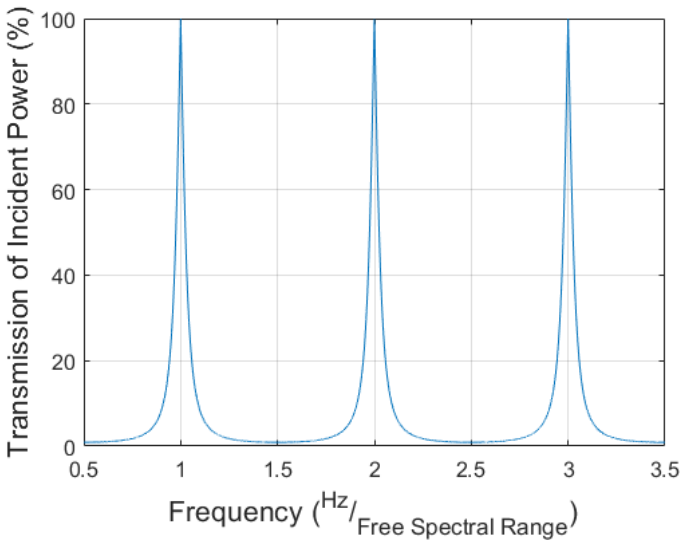

Figure 1.2. Simulated transmission spectra of a Fabry Pérot Cavity when Finesse = 50

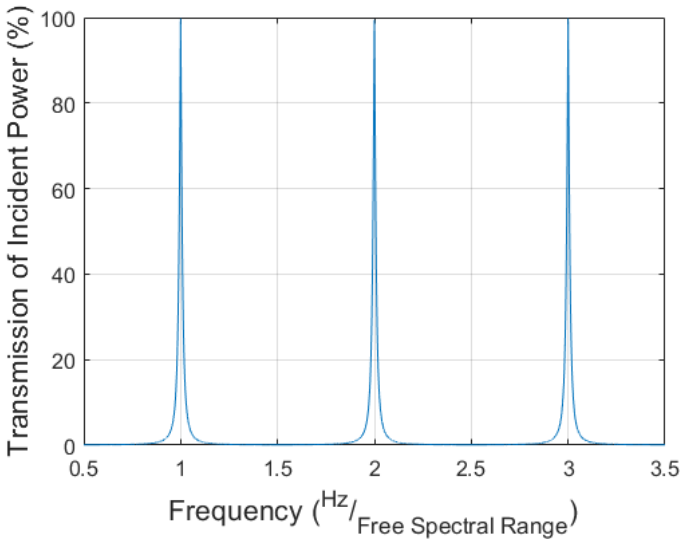

Figure 1.3. Simulated transmission spectra of a Fabry Pérot Cavity when Finesse = 150

be exactly 180° out of phase and destructively interfere, and the reflected beam vanishes[10]. This is why measured reflected power and the subsequent error signal power are zero as the pump sweeps over resonance. When the pump is deviated slightly off resonance, this phase relationship is either increased or decreased depending on which side of resonance the pump lies.

Now, when the incident light is phase modulated, the mismatch of this phase relationship to the sidebands is what generates an error signal when mixed down to DC. The mixer then takes the product of its two inputs.

$$A\sin(\omega_1 t)B\sin(\omega_2 t) = AB\frac{1}{2}[\cos((\omega_1-\omega_2)t) - \cos((\omega_1+\omega_2)t)] \tag{1.3}$$

In the PDH technique, $\omega_1 = \omega_2$, and the mixer frequency we are looking for will be at DC. For this, we use a Low-Pass Filter to isolate the $\cos(\omega_1 - \omega_2)t$ term:

$$\frac{AB}{2}\cos(\omega_1-\omega_2)t = \frac{AB}{2}\cos 0 = \frac{AB}{2} \tag{1.4}$$

So at its maximum, $\frac{AB}{2}$ will be our DC signal, isolated by a Low-Pass Filter. When these two signals are separated in phase, the amplitude of the DC signal is reduced. This can be seen in the extreme case when our mixer inputs are separated by 90°, represented by a sin and cos:

$$A\sin(\omega_1 t)B\cos(\omega_2 t) = AB\frac{1}{2}[\sin((\omega_1-\omega_2)t) - \sin((\omega_1+\omega_2)t)] \tag{1.5}$$

In this case, $\frac{AB}{2}\sin((\omega_1-\omega_2)t) = \frac{AB}{2}\sin 0 = 0$ is our filtered DC term. This is where a delay line or phase shifter is necessary to keep the phase difference of the two mixer inputs as close to zero as possible [10] [12].

In the absence of any phase matching, the amplitude of the error signal is determined by the length of each of the paths out of signal generator to the mixer. Referencing Figure 1.1, there will be some set time in each of the legs out of the signal generator. One path goes through the optical fiber, reflecting off of the cavity, and hitting a photodiode before the mixer. The other path goes from the signal generator straight into the mixer. Assuming the signal output from the signal generator will have a consistent velocity through each path, we can model this by giving a time delay to each leg, informed by the distance and velocity of each respective path. Our mixed input signals now become:

$$A\sin[\Omega(t+\tau_1)] \times B\sin[\Omega(t+\tau_2)] \tag{1.6}$$

Where Ω is the signal generator output frequency. Now, we have two mixer inputs whose phase relationship will now change with the chosen frequency of modulation Ω if $\tau_1 \neq \tau_2$. This means our DC signal amplitude will also be a function of Ω without any phase matching methods.

Additionally, the error signal's shape is dependent upon the modulation frequency used. If the phase modulation applied is smaller than the linewidth of the cavity resonance, then the error signal will have a more gradual slope between its maximum and minimum. This is due to the sidebands not being totally reflected back to the mixer. In the opposite case, when the frequency is high, or well outside of the linewidth of the cavity resonance, then the error signal will have much sharper peaks as the sidebands have a greater influence on the resultant DC signal.

Figures 1.4 and 1.5 are simulated error curves of a PDH technique. The x-axis is normalized for a resonance to occur every integer, and the y-axis is normalized so that the DC error signal is a function of the ratio of the pre-mixed RF signal from the photodiode and the light incident upon the cavity. Modulation frequency is set to 18 times greater than the resonance linewidth in the "High" modulation case, and the modulation frequency in the "Low" modulation case is set to the resonance linewidth. The simulated cavity has a Finesse of 300.

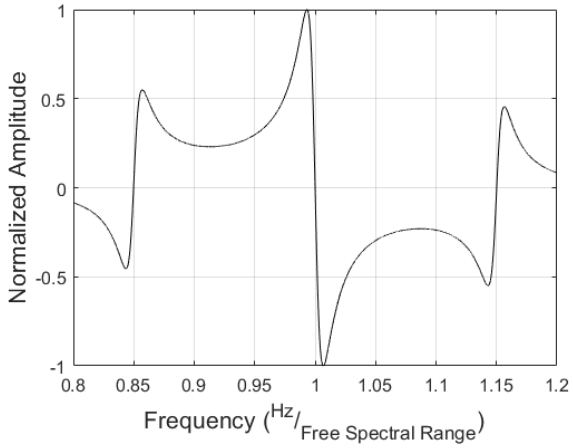

Figure 1.4. Example of a Pound-Drever-Hall Error Signal with 'high' modulation frequency. The modulation is about 20 linewidths of the resonance.

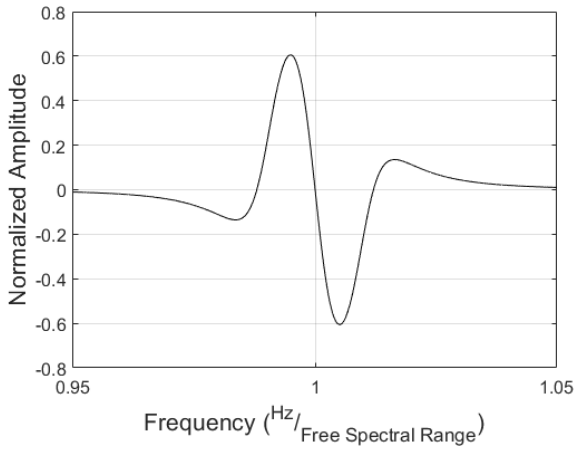

Figure 1.5. Example of a Pound-Drever-Hall error signal with 'low' modulation frequency. The modulation is about the same as the linewidth of the resonance.

Either way, the resultant error signal can be used in a feedback loop to keep the pump locked to resonance. The quality of the lock is then dependent upon the feedback control and the quality factor of the cavity.

1.2 Frequency Combs

Optical clock systems currently rely on generation of Optical Frequency Combs (OFCs). OFCs are frequency spectra that contain discrete, equally spaced lines in the frequency domain. OFCs to support atomic clocks were first introduced in 2000[3]. Prior to this, using optical frequencies in support of clocks was challenging due to their high relative frequencies. However, OFCs can overcome this challenge by creating signals that are directly convertible to the microwave domain, and vice versa.

Originally, an OFC is the result of a phase-stabilized Mode-Locked Laser (MLL). Modes inside the pulses of the MLL are coherent and equidistant in frequency. This means that knowledge of one mode is enough to know the frequency of any other mode. The two factors that control the resultant frequency comb is the repetition rate f_r and the carrier offset frequency f_{CEO}, where the frequency of any mode f_n, can be determined by $f_n = nf_r + f_{CEO}$, also known as the comb equation. f_r is controlled by the pulse-to-pulse timing of the MLL,

which also controls the spectrum of the OFC. In a static MLL cavity, the phase offset (Which informs f_{CEO}) of each pulse can be attributed to the properties of the laser cavity, and this is shown with the equation of $T = \frac{v_g}{2L}$ where v_g is the cavity's mean group velocity, T is the round-trip time of the light in the cavity, and L is the Length of the cavity[13]. The shorter the pulse, the broader the resulting OFC will be in the frequency domain[3]. A broad, octave spanning OFC is required for heterodyne beat detection, which results in f_{CEO} detection. Detection and stabilization of f_{CEO} is critical in optical clock systems. The spectrum of the OFC generated from an MLL is not stable on its own, and needs a stable reference to measure against. This can be done by comparing a difference frequency Δf generated from the OFC and locking it to a stable microwave reference. This method is not without its own challenges, as the stability of the OFC is now tied to the stability of its reference. The power to transition between the optical and microwave domains allows for a wider availability of references with greater stability.

In order to understand how to create an accurate optical clock, it is necessary to start with the comb equation:[14]

$$f_n = nf_r + f_{CEO} \tag{1.7}$$

Each of these frequencies will have a certain amount of instability associated with each of them [15]. So:

$$f_r = \hat{f}_r + \delta f_r(t) \tag{1.8}$$

$$f_{CEO} = \hat{f}_{ref} + \delta f_{ref}(t) \tag{1.9}$$

Where $\hat{f}_r$ and $\hat{f}_{CEO}$ can be considered stable, constant values. If a mode can be found to lie close enough to a reference, where $\Delta f = f_{ref} - f_n$, f_n can be locked to the reference. Assuming Δf is relatively small, the comb equation becomes:

$$f_{ref} \approx nf_r + f_{CEO} \tag{1.10}$$

Where f_{ref} has its own instability:

$$f_{ref} = \hat{f}_{ref} + \delta f_{ref}(t) \tag{1.11}$$

It should be noted that $\delta f_{ref}(t)$ will be relatively small, provided a highly stable reference is used, such as an atomic transition. The comb equation can be rewritten again to:

$$\hat{f}_r + \delta f_r(t) = \frac{\hat{f}_{ref} + \delta f_{ref}(t) - \hat{f}_{CEO} - \delta f_{CEO}(t)}{n} \tag{1.12}$$

Removing the constants from the equation, we are left with:

$$\delta f_r(t) = \frac{\delta f_{ref}(t) - \delta f_{CEO}(t)}{n} \tag{1.13}$$

And since n, the mode corresponding to the reference lock, is a physical property of the setup, it will be constant throughout the clock operation. Since $\delta f_{ref}(t)$ will already be small, locking f_{CEO} will reduce $\delta f_{CEO}(t)$, and will result in reducing $\delta f_r(t)$. Reducing $\delta f_r(t)$ in turn will provide a more stable comb. This explains why detecting and controlling f_{CEO} is important for building a reliable optical clock.

An advantage of microresonators is the ability to generate an octave spanning OFC with much lower power than an MLL. However, since OFC formation requires significant detuning of the pump laser away from the resonant mode of the microresonator, efficiencies of OFCs from microresonators are relatively low when a broad-spectrum OFC is needed[16]. For other applications, such as communications, microresonators with separate dispersion properties may be leveraged, such as dark pulse generation, which utilizes higher efficiency and a relatively narrowband comb[17].

1.2.1 Soliton Generation

Microresonators can only generate OFCs due to unique physical properties. Creation of the OFC requires a balance of the dispersive properties of the medium, the strength of the Kerr nonlinearity of the medium, as well as parametric gain and cavity loss. The

resultant OFC generated in this manner is known as a Dissipative Kerr Solitons (DKS). The sidebands that form the DKS occur when the parametric gain overtakes the cavity decay. When these sidebands are spaced in frequency equal to that of a single FSR, then the cascade of sidebands creates an OFC that is coherent [18]. This coherent comb can then be used in a similar fashion to the OFCs generated by MLLs, with the advantage of having on-chip comb generation, as well as broadband and octave spanning OFCs for a relatively smaller power investment.

1.2.2 Pound-Drever-Hall and Comb Applications

The PDH technique is useful when a laser's frequency relies on being stably locked to a cavity or resonator (typically with a higher Quality Factor than the laser cavity). In gravitational wave detection, a pump laser must be frequency stabilized to create a reliable interferometer setup[19]. This stabilization can be accomplished with the PDH method. In the case of optical timekeeping, a pump laser must be locked to a reference to reliably output a stable clock signal. This has already been demonstrated using the PDH technique on silicon-chip microresonators. Using the PDH technique in this way provides another tool to use in the implementation of optical clock architecture that can be installed on mobile platforms, such as ships or satellites[20].

Current clock architectures rely upon atomic microwave references such as the Caesium transition or rubidium atomic frequency reference, with the latter installed on the Galileo satellite network. The most compact state of the art clocks can take up a few liters of space on their local platform as well as needing about 35 W for operation [21] [4]. Instabilities in these microwave clocks are on the order of 10^{-12} for short integration times (1-10 seconds), in addition to long term drifts around 10^{-10} over the span of a year. Conversely, state of the art optical clock systems have been shown to have instabilities on the order of 10^{-14} to 10^{-16} over short integration times, with long term instabilities expected to be orders of magnitude lower than microwave counterparts. This improvement in time instability comes with the trade-off of more complex systems, with the best modern optical clocks needing several high-stability lasers, vacuum chambers, and complicated pre-operation calibrations.

In relation to Size, Weight, and Power requirements for optical clocks, volumes required start around 15 liters of space, with up to 1000 liters depending on the accuracy and complexity required, with powers at least an order of magnitude higher than microwave clocks [4].

Utilizing microresonators for OFC generation is only one step in moving optical clock systems toward miniaturization. Microring cavities today, such as the ones generated in silicon nitride, have the capacity to be utilized on chip, and require powers under a Watt to produce broadband OFCs. This is in contrast to broadband OFCs generated by Mode-Locked Lasers that would require of tens of watts while needing hundreds of liters of space to operate. Future efforts to reduce size and power requirements for a fully realized optical clock system involve miniaturization in other active optical components in order to approach the current size and power of state of the art microwave clocks.

Improvements in Global Navigation Satellite Systems (GNSS) or maritime operations will require the advancement of this miniaturization. Improving the robustness and accuracy of GNSS will require either compactness in optical clock systems, or large improvements in communication and time syncing between satellites[4]. Communication networks in use today also rely on accurate time keeping with Time Division Multiple Access, requiring constant syncing with their network to reduce dead time on a used frequency. Better local or centralized timekeeping with greater accuracy will allow for more robust communications and data transfer. [22][23] In the case of silicon-based microrings, the PDH technique can even be used as a form of thermal response characterization[24], in addition to larger locking schemes.

2. EXPERIMENT 1: CONTINUOUS WAVE LASER TO FABRY-PÉROT CAVITY

This experiment sought to lock a continuous wave laser to the resonance of a Fabry-Pérot Cavity using the PDH technique. The pump laser was phase modulated before passing through a circulator and through a Fabry-Pérot Cavity (FPC). The reflected light was then sent back through the circulator and mixed to DC where an Error Signal was used to lock the system via the Laser's Piezoelectric Transducer (PZT) control.

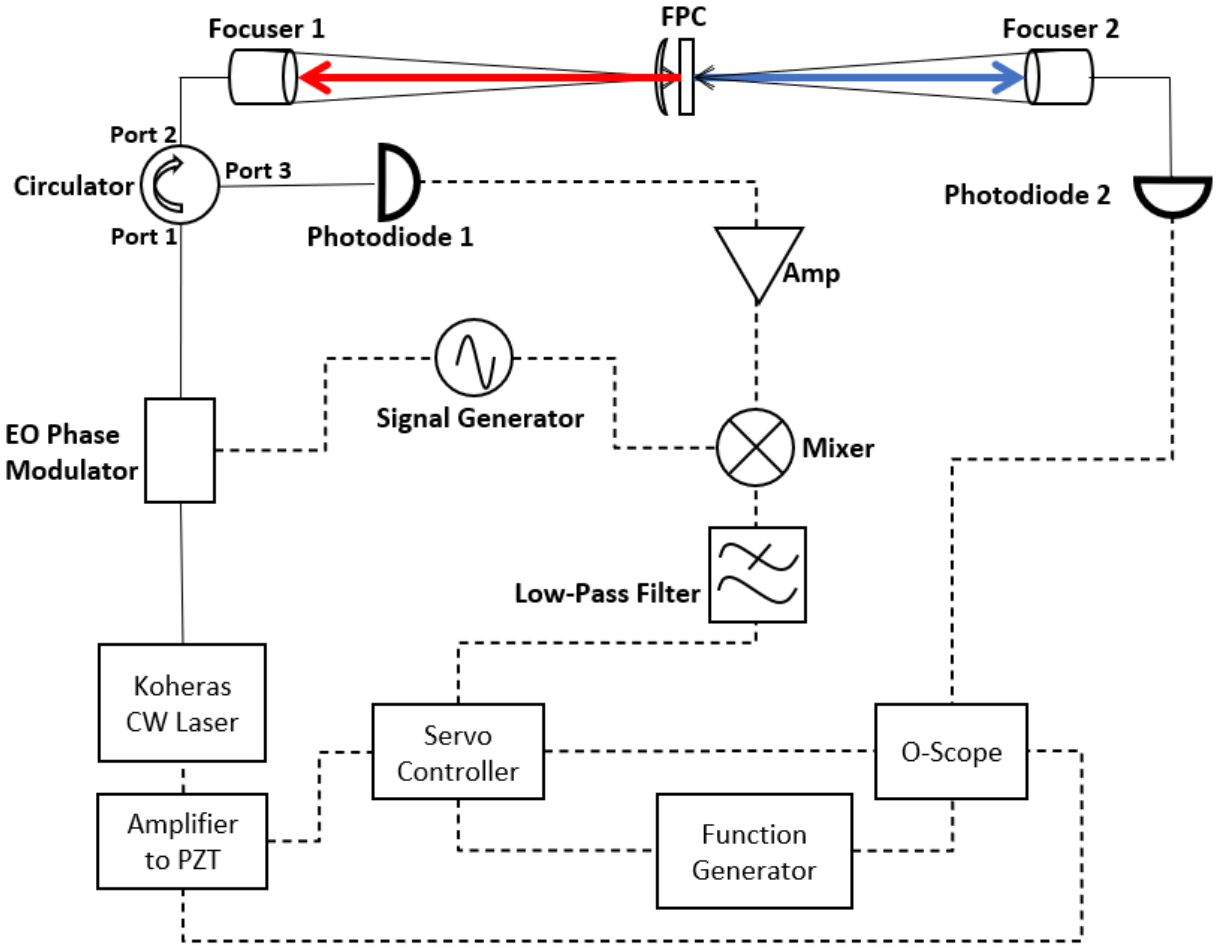

Figure 2.1. Experimental setup of the Pound-Drever-Hall technique using a Fabry-Pérot Cavity

2.1 Methods

2.1.1 Focuser-Cavity Coupling

Prior to the Pound-Drever-Hall setup that was used in Figure 2.1, I needed a way of coupling the pump light to the cavity. A Koheras Adjustik laser was used as the pump laser, at an output of 16 mW through 1.5 μm optical single-mode fiber. This pump light then passed through a ThorLabs 3 port circulator. The circulator was needed to transfer reflected light coming back from the FPC into port two and out to the mixer via port 3 to a ThorLabs power meter. Following the output of port 2 of the circulator, the light was emitted out of a focuser mounted on a stage and rail system capable of 3D translation, pitch, and yaw adjustments. Figure 2.2 is an image of these components with their mounts and rail system. It is expected that free space collimators would have been acceptable substitutes to couple light into the FPC. The focusers and cavity were used because they had been demonstrated to couple previously in the same lab [25] [26].

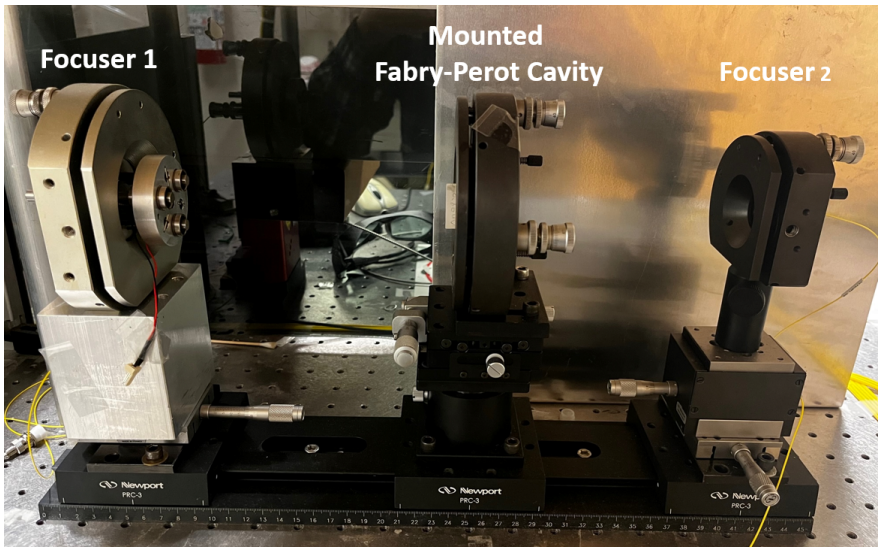

Figure 2.2. Image of focusers with mounted Fabry-Pérot Cavity

Focuser 1 had a rated magnification of 38 at a working distance of 25 cm and Focuser 2 had a rated magnification of 40 at a working distance of 25 cm. Coupling to the cavity was accomplished by procedures originating from experiments performed by Dr. Dongsun Seo and Dr. Daniel Leaird [25] [26]. First, both focusers were placed across from each other

at a distance of 32 cm. At optimum alignment, insertion loss had been measured to be 0.5 dB at a distance of 32 cm. The focusers' heights and horizontal positions were matched by eye, and verified by using infrared sensor cards. The tilt of Focuser 1 was adjusted to minimize insertion loss, and then the tilt of Focuser 2 was adjusted to minimize insertion loss. Following this, small adjustments in heights, distance, and horizontal positions were then made starting with Focuser 1 before adjusting Focuser 2 to further minimize the insertion loss.

Next, the flat cavity facet was located and placed in the center between the two focusers facing Focuser 2. The flat cavity was determined outside of the setup using a collimator emitting infrared light and observing the promptly reflected beam using an infrared sensor card. This was done to minimize the transmitted free-space beam area to Focuser 2. Conversely, it was expected the small amount of refraction from the 500 mm radius curved facet that would affect the reflected beam would be acceptable coupling loss, as the reflected beam from the FPC into Focuser 1 was expected to have a higher amplitude than the transmitted beam into Focuser 2 in all cases except when the pump fell within the linewidth of a resonance. The setup shown in Figure 2.3 was used for the coupling. Next, the tilt of the mounted FPC was adjusted to maximize the reflected power measured at Power Meter 1.

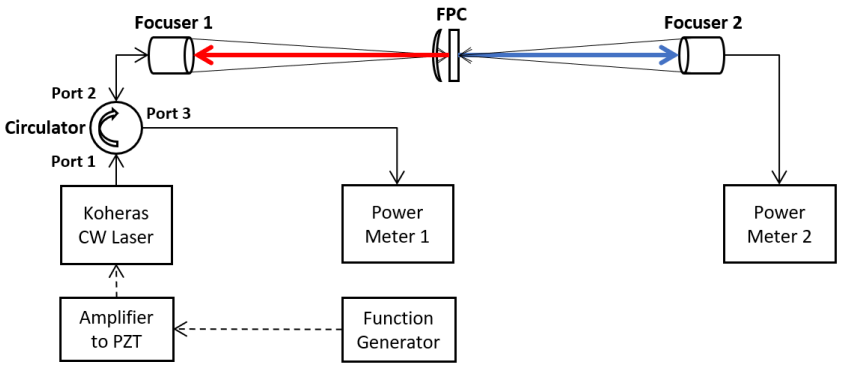

Figure 2.3. Setup for coupling to the Fabry Pérot Cavity

Next, a Wavetek 182A function generator was turned on to start the pump's PZT sweeping. The function used was a 100 Hz ±10 V saw tooth function which was them amplified by

the PZT amplifier to produce a ≈3 GHz sweep from the pump, using the Koheras Adjustik specifications and voltmeter measurements output by the amplifier.

Following this, an infrared sensor card was placed between the FPC and Focuser 2, to check if the pump was sweeping over a resonance. The pump's cavity was thermally tuned until light was visible on the infrared sensor card. At Focuser 2, the sensor card was expected to show a line due to mode mismatching. The horizontal position on the FPC was then adjusted to orient the line displayed on the sensor card in a vertical position. Next, the vertical position of the FPC was adjusted to shrink this line to a point.

Finally, small adjustments to the tilts, heights, distances, and horizontal positions of the two focusers were made until Power Meter 1 was displaying a maximum with sweeping off, and Power Meter 2 was displaying a maximum with sweeping on. With this, the Focusers were considered coupled to the Fabry-Pérot cavity.

2.1.2 Setup

Following the coupling process, the setup in Figure 2.1 was constructed. The pump was phase modulated by an EOSpace Lithium Niobate Electro-Optic Phase Modulator (EOPM) with a $V_{\text{pi}} = 3.0@1\text{GHz}$ before passing through port one of a the circulator. The phase modulation, being a key component of the PDH technique, is necessary to establish the phase relationship that occurs between the first and second mirror. Interfering these side bands with the reflected pump beam is critical to the error signal generation [10]. In the full setup, the circulator was needed to transfer reflected light coming back from the FPC into port two and out to the mixer via port 3 for generation of the error signal. Both photodiodes used were Agere 2560A-C02 models, rated at 12 GHz bandwidth. The photodiodes were more than sufficient, as it was expected to only need a photodiode bandwidth greater than the applied phase modulation frequency. Following the RF output of Photodiode 1, the signal was amplified by a Mini-Circuits ZFL-500LN amplifier with a measured gain of 28 dB before entering the RF input of a Mini-Circuits ZEM-2B+ mixer. The LO input of the mixer was the same RF signal that was used in optical phase modulation, and was generated using an HP8648C signal generator set at 184 MHz with an ouput power of 10

dBm. Splitting the output of the signal generator incurred about 3 dB of loss to each branch, resulting in ≈7 dBm reaching the EOPM and mixer each. The output of the mixer was filtered using a Mini-circuits BLP-100+ low pass Filter with a 3-dB corner at 108 MHz before entering a New Focus LB1005 servo controller (servo). This low pass filter ensured the DC component of the mixed RF signals would dominate. A lower-frequency corner filter could have been used, but a low-pass filter with its frequency corner below the modulating frequency output by the signal generator was seen to have the best effect. The output of Photodiode 2 was sent directly to an oscilloscope as another check for when the pump was operating at the FPC resonance, and was later used to verify the system was locked and remained at resonance. The FPC was a 15 mm air-spaced concave mirror followed by a flat mirrors with $0.01\frac{ppm}{^\circ K}$ temperature dependence. Curvature of the concave incident mirror was 500mm, and the Finesse was rated at 270. The servo received the output of the mixer as well as the output of a function generator, set at a 100 Hz symmetrical ramp function at an amplitude of ±10 V. The servo output the frequency of the Wavetek function generator, with an amplitude of ±10 V. The servo had an available setting attenuating the amplitude of the sweep function, effectively reducing the sweep range. During a lock, this sweep range was completely attenuated, outputting a constant voltage value within the servo's input range determined by the Wavetek function generator (i.e. the ±10 V input). The servo then maintained a 0 V error signal input by outputting a corresponding DC Voltage within the ±10 V range. This output is described as:

$$V_{output} = V_{control} + V_{center} \tag{2.1}$$

Where V_{center} is the adjustable offset of the sweep function amplitude, and:

$$V_{control} = V_{error}\frac{K2\pi f_{PI}}{s}(1 + \frac{s}{2\pi f_{PI}}) \tag{2.2}$$

Where V_{error} is the absolute difference between the servo's input voltage and zero, K is the set proportional gain of the servo, s is the input sweep frequency from the function generator, and f_{PI} is the 3-dB break frequency above which proportional gain K dominates over the servo's integration gain.

An input offset setting is available in the case of locking to a swept signal that is nonzero, but was not used for the PDH experiments. The output of the servo was then sent to an input on a Piezo System Inc. EPA-104 linear amplifier that was connected to the PZT of the Koheras laser. The PZT has a rated range of ±200 V, but a range of only ±52.5 V, measured with a voltmeter, was used to avoid any damage to the laser system. Using the laser specifications, this left an expected range of ≈1575 MHz as the PZT was swept using the linear amplifier with a rated input of ±10 V from the function generator. This means that the linear amp was operating with a gain of about 5.25. The oscilloscope inputs were the function generator used as a sync, an input repeater from the servo (known as the error monitor output), and Photodiode 2 output. The oscilloscope used was a Keysight DSOX3024A with 350 MHz bandwidth. Table 2.1 lists important parameters.

Using this setup, the PZT input was left to oscillate between ±52.5 V, while the laser was thermally tuned in expectation the pump would fall within of a FPC resonance during the sweep. Performing a sweep in this manner allows for the viewing of photodiode response over the sweep range, which informs the tuning necessary of the pump before the lock is engaged. The laser's cavity was capable of being tuned from 15.0°C to 50.0°C with a thermal tuning coefficient of $9.4\frac{pm}{^\circ K}$. This leads to the estimated thermal tuning range of ≈41.5 GHz, referencing the measured specified wavelength of 1541.9 nm at 35.0°C. With an anticipated thermal tuning range of 41.5 GHz, it was expected to find multiple resonances across the laser's full tuning. The resonance found and utilized for locking was found at a temperature of 22.1°C. Subsequent resonances were found at temperatures 30.5°C, 39.0°C, and 47.7°C. These resonances approximately coincided with an estimated 10 GHz shift for every 8.4°K of thermal tuning. In the absence of a resonance, or when the pump laser detuning was greater than the sweeping range of the PZT, both the error monitor and Photodiode 2 output registered nearly 0 V on the oscilloscope for the entire sweep time of 10 ms. When a resonance was close (within $\frac{1575}{2}$ MHz of the pump), an error signal was seen as well as a transmission spectra from Photodiode 2.

Figure 2.4 shows the responses when the PZT was swept across the range supplied by the linear amplifier. The pump was tuned close enough to the FPC resonance that transmission both on resonance and the phase modulated sidebands are visible during the PZT sweep, as

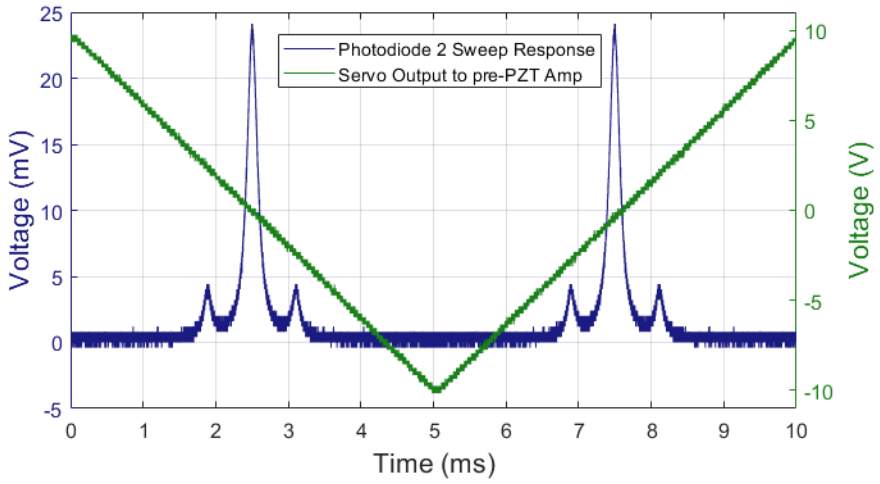

(a)

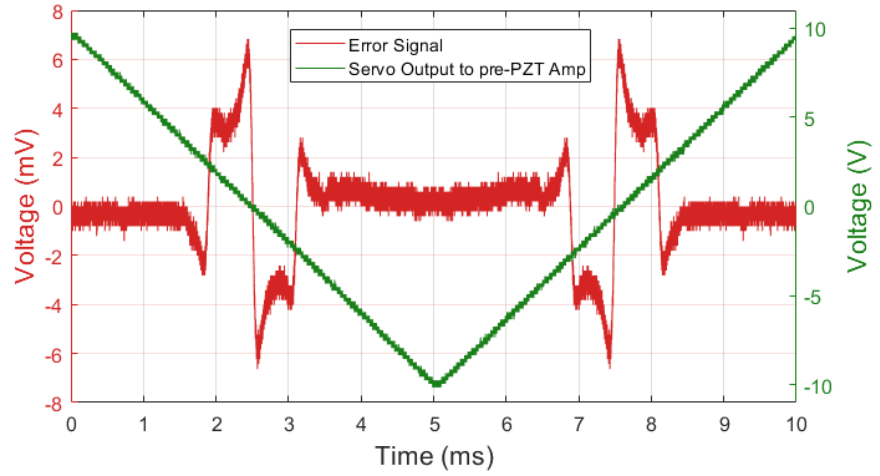

(b)

Figure 2.4. (a) Photodiode 2 response during Piezo sweep (b) Servo input during Piezo sweep

shown in Figure 2.4a. The DC signal from the Mixer that is input into the servo is repeated at the servo's error monitor output, shown in Figure 2.4b. This is the PDH error signal, and was used by the servo for locking.

Once the pump was sufficiently close to FPC resonance, the sweep amplification was lowered while keeping resonance within the reduced sweep. This included the center zero crossing point of the error signal. Sweeping was then turned off and the servo lock was engaged with settings at $f_{PI} = 100\text{Hz}$, $s = 100\text{Hz}$, and $K = 3.4$. The servo then maintained

the pump on resonance by adjusting its output signal to the pump PZT, and was held in place for an hour.

Table 2.1. Pound-Drever-Hall technique using Fabry-Pérot Cavity Parameters

Parameters	Value
CW Laser P_{out}	12 dBm
CW Laser Drift	$8.8\frac{MHz}{min}$
Cavity Coupling Loss	5 dB
Low-Pass Filter 3-dB Corner	108 MHz
Signal Generator $f\&P_{out}$	184 MHz @ 10 dBm
Amplification Gain	28 dB
PZT Sweep Frequency	100 Hz
FPC First Mirror Radius	500 mm
FPC Second Mirror Radius	∞m
FPC Free Spectral Range	10 GHz
FPC Finesse	270

2.2 Results

Prior to locking, the swept signals were needed for reference and are shown in Figure 2.5. Using the peak power of the sidebands, the rate of $\frac{\text{Hz}}{\text{ms}}$ can be calculated, and checked with the estimated Δf of the entire sweep. Figure 2.5 shows this relationship by setting the origin of the x-axis at FPC resonance, and using the known 184 MHz sidebands to construct the Δf relationship of the sweeping spectra.

Figure 2.6 shows the response of the locked laser over one hour. The lock was confirmed by referencing the power levels of transmission as the laser swept over FPC resonance over one hour. As shown by Figure 2.6, the transmission power remained at resonance levels throughout lock engagement, demonstrating that the laser was maintaining a frequency consistent with the FPC resonance throughout. Between 300 to 600 seconds during the experiment, the system was unlocked to again reference the power of transmission and reflection. This unlocked state appears to show the pump outside resonance, with a much smaller amount of power output from Photodiode 2, or FPC transmission.

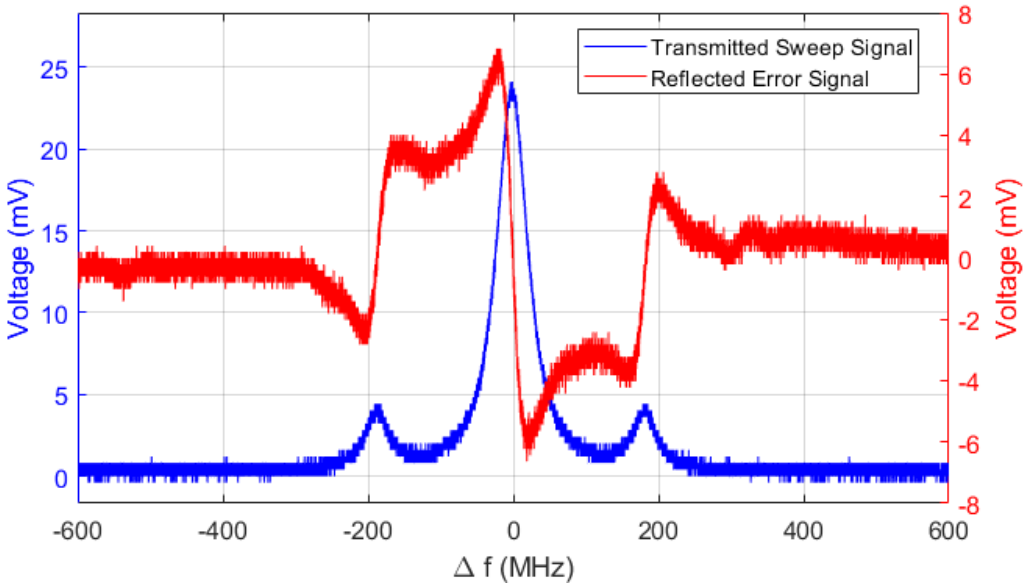

Figure 2.5. Fabry-Pérot Cavity transmission and reflection while sweeping pump Piezo

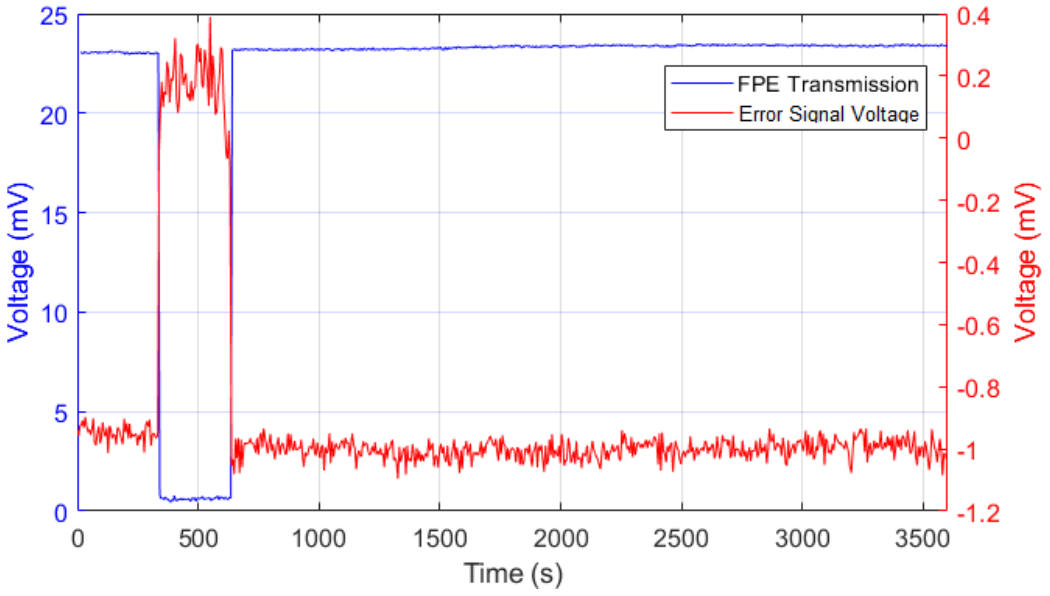

Figure 2.6. Fabry-Pérot Cavity transmission and reflection with servo lock engaged

3. EXPERIMENT 2: CONTINUOUS WAVE LASER TO 25 GHZ FREE SPECTRAL RANGE MICRORING

This second experiment sought to lock a continuous wave laser to the resonance of silicon nitride microring resonator with a rated Free Spectral Range (FSR) of 25 GHz. While using the same laser from the first experiment, it was important to use a relatively low FSR ring because the laser only had a tunable range on the order of 41.5 GHz. This guaranteed that at least one resonance would fall within the tuning range of the laser. Additionally, a Vector Network Analyzer with an additional Electro-Optic Phase Modulator was used to measure the difference between pump frequency and the microring resonant frequency. A table of experiment parameters can be found in Table 3.1.

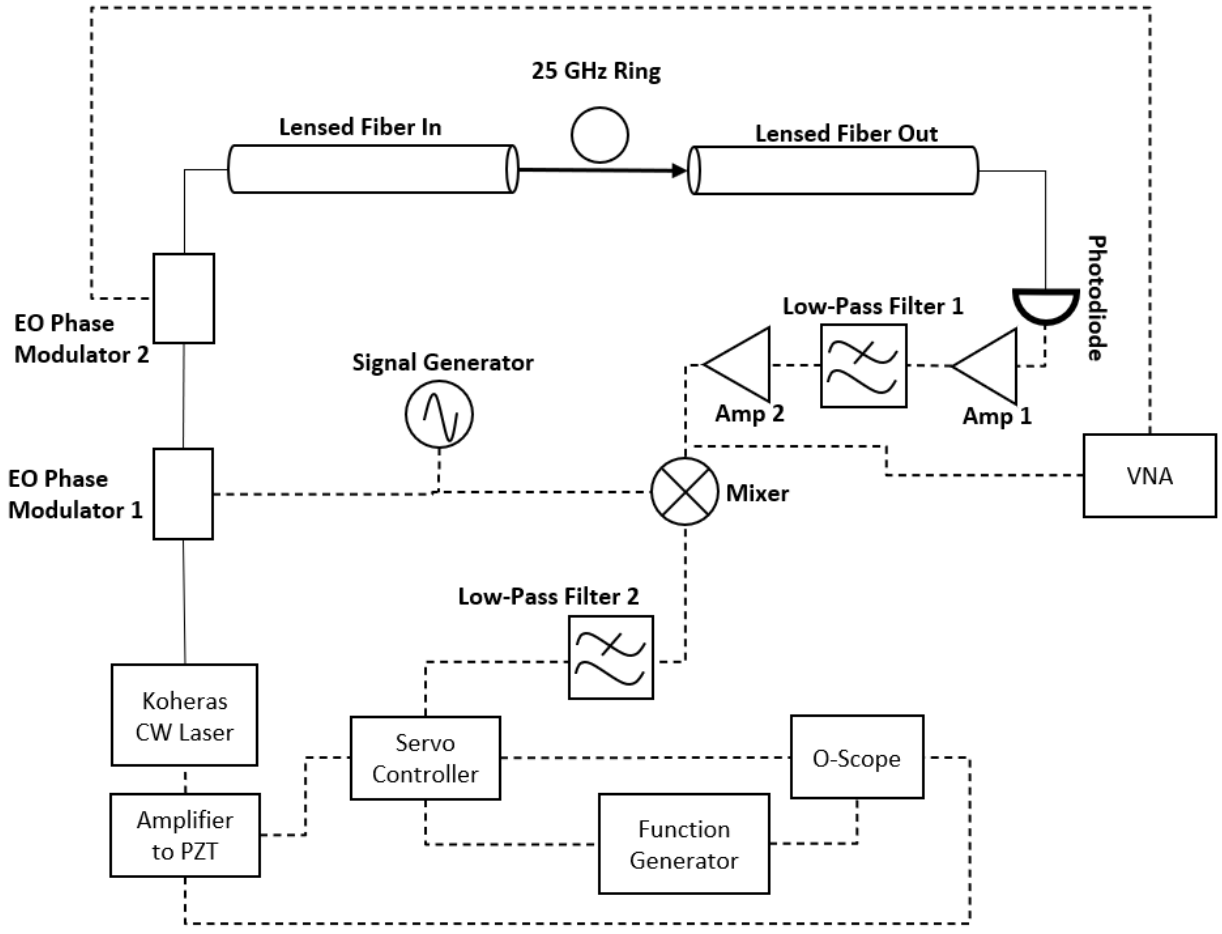

Figure 3.1. Experimental setup using a 25 GHz Free Spectral Range microring cavity

3.1 Methods

The same Koheras Adjustik laser used in Experiment 1 was used in this experiment. The output power was 100 mW through 1.5 μm optical single-mode fiber. The light was phase modulated by an EOSpace Lithium Niobate Electro-Optic Phase Modulator (EOPM) with a $V_{pi} = 3.0$@1GHz with an input frequency of 294 MHz to establish the phase relationship between light on either side of resonance in the frequency domain using the sidebands. A second EOSpace Lithium Niobate EOPM (also with a $V_{pi} = 3.0$@1GHz) was placed in series with the first, with its input connected to an Agilent N5230C Vector Network Analyzer (VNA). The VNA was operated by sweeping a frequency between 300 kHz and 1 GHz, and recording its S_{21}, or forward gain received as it swept across the frequency spectra. This was used to establish the microring resonance in relation to the pump frequency. As the VNA performed its frequency sweep, it created additional sidebands on both the pump frequency and EOPM 1's sidebands. As these sidebands swept over resonance, an RF response at the input frequency is expected to be detected by the photodiode due to the phase difference created between the sidebands. Additionally, this RF signal should be the same frequency as the phase modulation. Since the pump was expected to be much more powerful than the EOPM 1 sidebands, sidebands generated by EOPM 2 on the pump were expected to dominate. This is how the VNA was used to measure distance between pump and resonant frequencies. Following EOPM 2, the light was coupled into the 25 GHz FSR ring by lensed optical fibers before hitting a photodiode. The ring was mounted on a vacuum stage and coupled using the mounted lensed fibers. The mounts were capable of 3D translation, pitch, and yaw adjustments. An image of the ring is shown in Figure 3.2. An image of the mounting stage is shown in Figure 3.3.

Coupling light into the microring was more straightforward than the free space focusers used in Chapter 2. The experiment shown in Figure 3.1 was constructed, and a ThorLabs optical power meter was installed at the output lensed fiber. The lensed fiber ends were then translated close to the bus waveguide input and output of the microring. Following this, adjustments were made one lensed fiber at a time to maximize output power through the

bus waveguide. All of the adjustments and lensed fiber positions were visually monitored using a ThorLabs Kiralux camera mounted on a magnification apparatus.

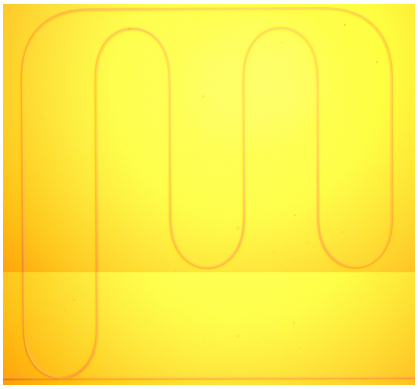

Figure 3.2. Image of the 25 GHz Free Spectral Range microring resonator

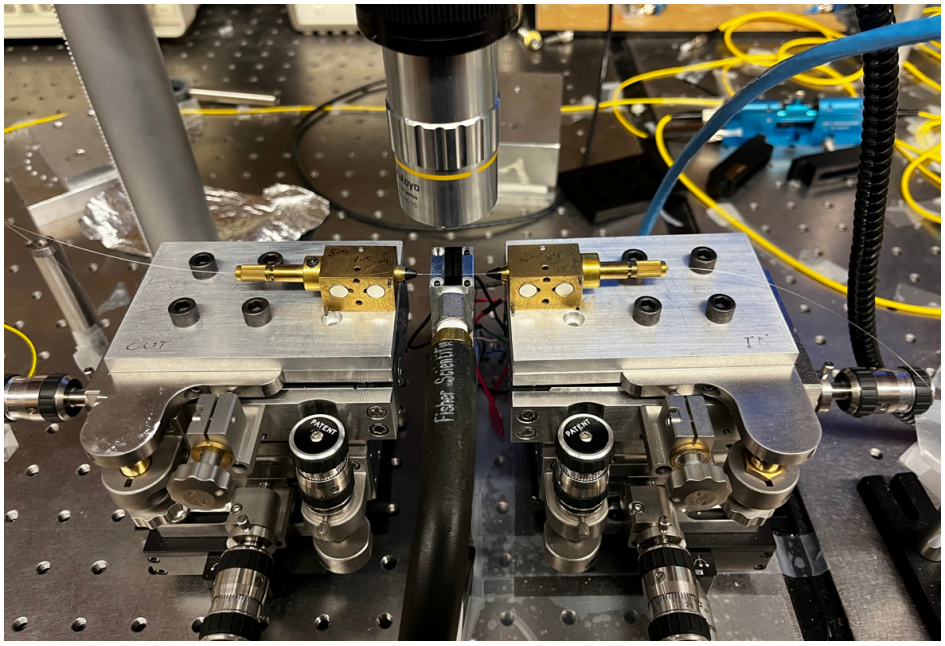

Figure 3.3. Image of coupling stage with lensed fibers

Filtering was performed prior to the mixer because the primary frequencies of interest were those used to modulate in EOPM 1 and EOPM 2. More amplification was needed than in Experiment 1 due to the anticipated insertion loss of including a second EOPM and splitting the RF signal prior to mixing. Two amplifiers were used, where Amp 1 was Mini-Circuits ZFL-1000LN+ and Amp 2 was ZFL-500LN, with rated bandwiths of 0.1-1000

MHz and 0.1-500 MHz respectively. Low-Pass Filter 1 was a Mini-Circuits SLP-450+ with a 3-dB corner at 440 MHz. Any signal above 500 MHz was expected to be dramatically attenuated due to the filter and amplifier bandwidth.

Following this amplification and filtering chain, the signal was split between the mixer and the VNA. The input to the VNA was used in its S_{21} measurement, while the RF signal sent to the mixer was mixed with the same phase modulated RF signal of EOPM 1 using the ZEM-2B+ mixer and filtered using a BLP-100+ so that the DC signal would dominate. The signal generator used was the same HP 8648C. This DC signal was the input to the New Focus LB1005 servo controller (servo) that repeated its input to a Keysight DSOX3024A. An Agilent 33220A fuction generator was synced with the oscilloscope and output to the servo, outputting a ramp function with 1% symmetry at a frequency of 90 Hz. The servo output the same ramp function while sweeping the PZT. The 1% symmetry was used so that the observed frequency sweep of the PZT would occur in one direction (blue to red in the case of this experiment). This would ensure that any thermo optic effect experienced by the microring would be consistent across all observed sweeps. The ramp function taken from the function generator and output by the servo can be seen in Figure 3.4.

Table 3.1. Pound-Drever-Hall technique using a 25 GHz Free Spectral Range Microring Cavity Parameters

Parameters	Value
CW Laser P_{out}	20 dBm
Ring Coupling Loss	16 dB
Filter 1 3-dB Corner	440 MHz
Filter 2 3-dB Corner	108 MHz
Signal Generator f&P_{out}	294 MHz @ 10 dBm
Amplification Gain	40 dB
PZT Sweep Frequency	90 Hz
Microring Reported Q	$\mathcal{O} \sim 1.2 \times 10^6$@1550$nm$
VNA P_{out}	-5 dBm

Before utilizing any locking, it was important to establish the error signal input to the servo. When the servo output a sweeping function of ±10 V, the sweep of the PZT was found to cover a range of approximately 1560 MHz. This was calculated using the generated

sidebands, and confirmed by increasing the phase modulation frequency until the sidebands were at the edges of the PZT sweep. This meant the PZT was oscillating between -51.5 V and +51.5 V with a PZT amplifier set to 5.15, confirmed by using a voltmeter on the PZT amplifier output. A single sweep is shown in Figure 3.4, and occurred at 90 Hz.

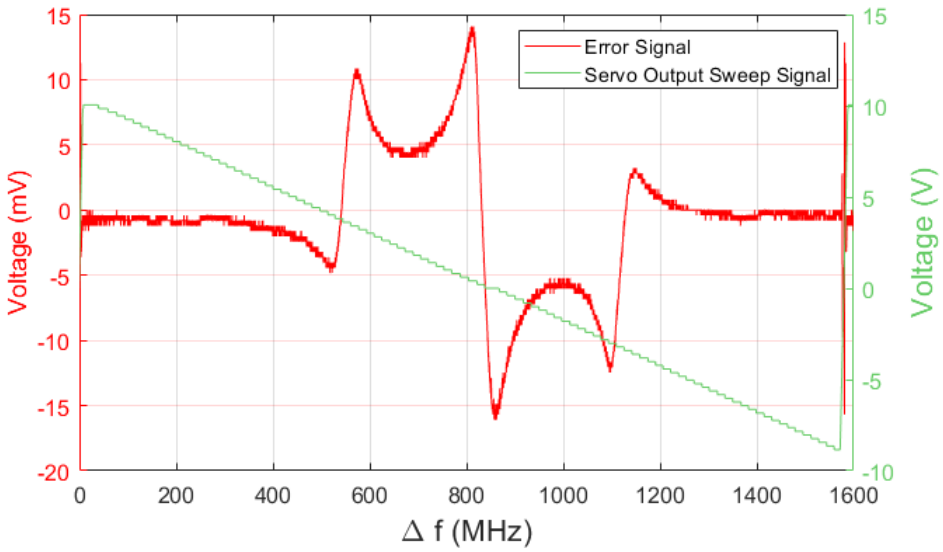

Figure 3.4. Error signal with sweep function

Next, the pump was thermally tuned outside of the PZT sweep range. Sweeping was then turned off, and the PZT voltage was set to zero. This meant resonance was at least over 780 MHz away from the pump when sweeping was turned off, as the 51.5 V sweep in either direction in frequency corresponded to 780 MHz away from a PZT voltage of 0 V. After turning off PZT sweeping, a S_{21} trace from 300 kHz to 1 GHz was taken, shown in Figure 3.5a. The S_{21} shows that when resonance is not close to pump frequency, the unfiltered gain is close to -50 dB. An elevated noise floor is expected due to the large amount of amplification needed prior to the VNA input.

This process was repeated with the pump thermally tuned as close to resonance as possible without engaging any locking. Another S_{21} trace was taken, and it shows a peak near 60 MHz on the order of -30 dB in Figure 3.5b. In the case where resonance was close to pump frequency, the laser cavity was set to 29.5°C. The S_{21} when a generated sideband has passed over resonance shows a RF response from the photodiode. This makes measuring

the distance in frequency between the pump and microring resonance viable. Of note, this does not indicate the direction of the difference (i.e. whether the pump is higher or lower in frequency to the ring resonance) but only the absolute distance between them in frequency.

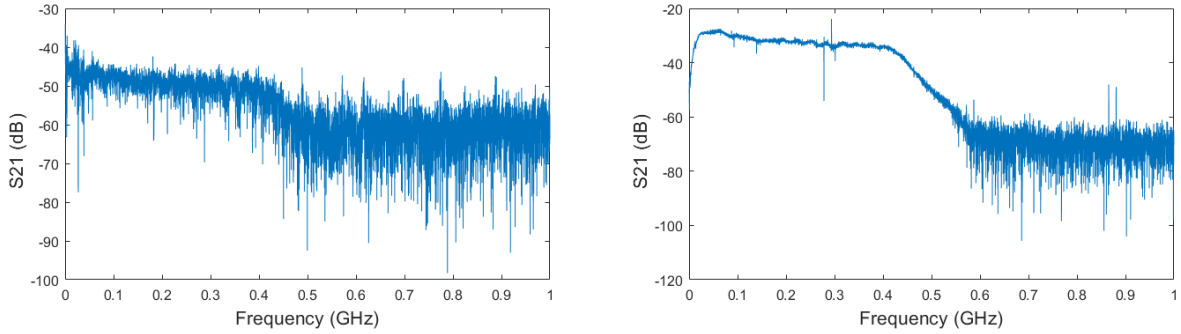

(a) (b)

Figure 3.5. (a) Vector Network Analyzer S_{21} with pump >780 MHz away from microring resonance. (b) Vector Network Analyzer S_{21} with pump close to resonance

Following this, the pump was tuned to an arbitrary point within 500 MHz of resonance and three VNA traces were taken over the course of an hour to observe drifting between the pump and resonator. In total, three traces were taken, one at $t = 0$ minutes, $t = 30$ minutes, and $t = 60$ minutes. These traces can be seen in Figure 3.6. Using peak S_{21} measurements taken from the VNA, the pump started at 252 MHz away from resonance, and ended at 61 MHz away after an hour. These three measurements do not establish any rate of drift, nor which device (microring or pump) is drifting more, but drift between pump and resonance is shown to exist with the changing frequency distance between pump and resonance over arbitrary time scales.

Additionally, VNA traces were taken while the pump was being thermally tuned. The pump cavity was set 29.5°C, corresponding the pump's frequency close to the microring's resonant frequency. Next, the pump cavity was increased in small increments to intentionally move the pump center frequency away from resonance. The smallest increment of temperature change ΔT was 0.1°C. Three small increment changes were made with the VNA measuring its S_{21} between pump cavity temperature changes, while recording the pump's reported internal cavity temperature. It was expected to see the S_{21} traces' peaks increase in

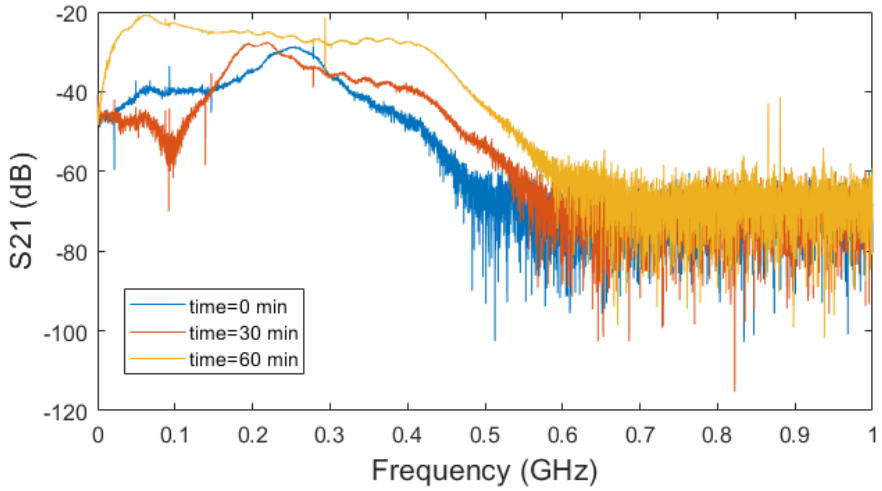

Figure 3.6. Vector Network Analyzer S_{21} over an hour in an unlocked system

frequency as the pump cavity temperature was changed. In this case, the ΔT was positive, but decreasing the pump cavity temperature would have had the same expectations.

The VNA was able to measure how far the the pump was tuning away from resonance before being attenuated by Low-Pass Filter 1 corner. As seen in Figure 3.7, the pump started close to 63 MHz away from resonance, and tuned about 430 MHz away from resonance in response to a 0.2°C shift in pump cavity tuning. When the pump was tuned further away from resonance, the pump-resonance distance appeared to widen past 500 MHz, where it was expected to be attenuated by the amplifier-filter chain.

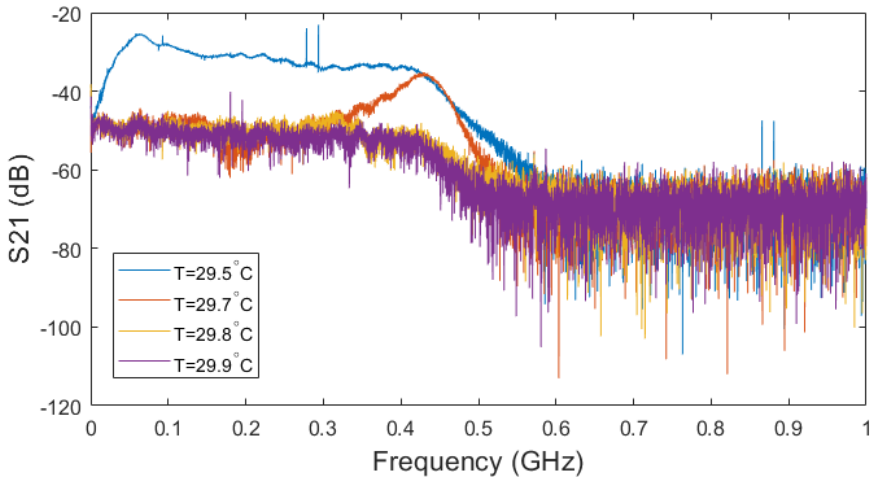

Figure 3.7. Vector Network Analyzer S_{21} with thermal pump tuning in an unlocked System

3.2 Results

The locking experiment was then engaged twice using PZT control via the servo. Servo settings were at $f_{PI} = 100$Hz, $K = 3.9$, and $s = 90$Hz. Equations 2.1 and 2.2 show the servo output logics.

First, the lock was left engaged for an hour and corresponding VNA S_{21} traces were taken at $t = 0$ minutes, $t = 30$ minutes, and $t = 60$ minutes. These traces can be found in Figure 3.8. All three traces appear to be similar in shape and amplitude. In each case, S_{21} shows a RF response from the photodiode starting at 24 MHz to 26 MHz. The S_{21} RF responses were between -29 and -27 dB. This means that there was positive RF signal from the photodiode over the range of a few MHz while the lock was engaged. In contrast to Figure 3.6, the S_{21} of a locked system indicates that the previous drift over time has been corrected for.

Finally, the lock was left engaged while the pump cavity temperature was tuned over a range of 0.5° C. The pump was frequency tuned away from resonance, but still within the PZT sweep range, at a pump cavity temperature of 29.3°C, and then increased 0.5°C, with a new S_{21} trace taken at 29.5°C and 29.8°C. These S_{21} traces are shown in Figure 3.9. There is detected RF response between 22 MHz and 24 MHz between all three traces. This indicates that even though the pump was changing its center frequency by tuning the laser cavity temperature, the servo controlling the PZT was correcting for this mismatch and keeping the pump output near resonance.

The pump cavity temperature range of $\Delta T = 0.5$°C was chosen based on the observations made prior to lock in Figure 3.7. It was known that the pump was observed to be close ($<$ 100MHz to resonance when the pump cavity temperature was set to 25.5°C. And since the pump frequency difference to the microring resonance shifted past 500 MHz between a 0.2°C and a 0.3°C shift in one direction, the range of 29.3°C to 29.8°C was chosen to reflect when the pump frequency was both above and below the resonant frequency. It is worth noting the temperature offset would only be able to continue as long as the difference in frequency between the pump and resonator could be corrected for by the PZT. Based on previous discussion and Figure 3.4, this would be around when the pump and resonance were 780 MHz apart in frequency with the PZT set to 0 V. Referencing the laser specifications as well as

the drift seen in Figure 3.7, this would be expected when the laser cavity temperature would have been $\approx 25.5°\text{C} \pm 0.5°\text{C}$. This range could be expanded by increasing the amplification of the servo's output to the PZT, so long as no over-voltage occurred. Based on laser PZT specifications, this range could be expanded to a 3.0 GHz difference in the pump cavity and microring resonance with the PZT at 0 V, corresponding to a $\Delta T \approx \pm 2.0°\text{C}$ temperature range when the pump cavity is thermally tuned close to resonance. Furthering this offset range even further would require a different, wider frequency tuning range capability than what was used in this experiment which could be remotely controlled.

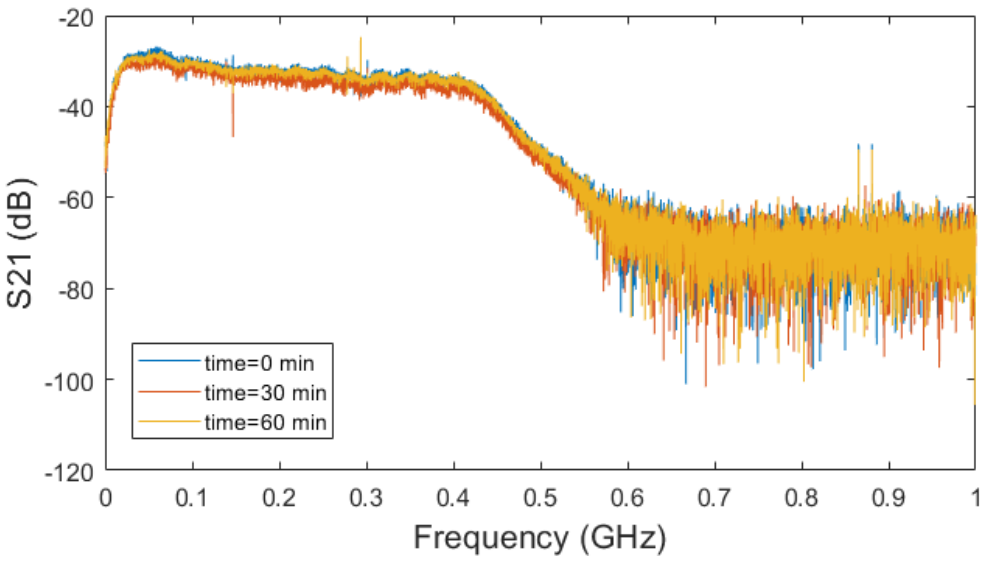

Figure 3.8. Vector Network Analyzer S_{21} over one hour in a locked system

These two instances of locking were used to indicate a lock was being maintained by the PZT control. All traces in Figures 3.8 and 3.9 share the S_{21} characteristics with a pump that is close to resonance in Figure 3.5b, and they are maintained both over time and when the pump is intentionally tuned away from resonance. From this I concluded that the PDH technique was accomplished on a 25 GHz FSR microring.

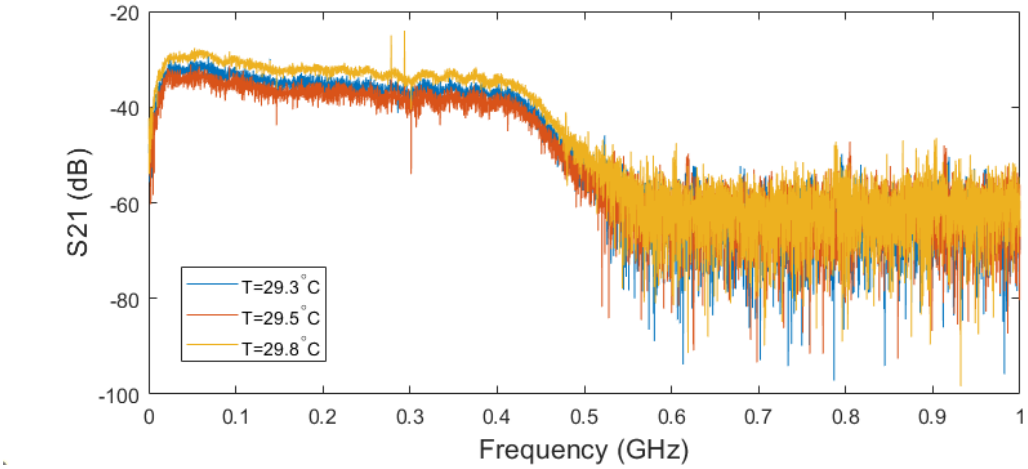

Figure 3.9. Vector Network Analyzer S_{21} with pump tuning in a locked system

4. EXPERIMENT 3: 890 GHZ MICRORING COMB APPLICATIONS

This third experiment sought to establish the PDH technique to a microring that was generating a broad Optical Frequency Comb. The work in this experiment was work done in collaboration with lab members Nathan O'Malley, Saleha Fatema, and Dr. Kaiyi Wu. First, we demonstrated a lock of the pump to the microring with a Free Spectral Range (FSR) of 890 GHz. The PDH technique was accomplished by using a continuous wave laser which was sent through a Single Sideband Modulator (SSM) controlled by a Voltage Controlled Oscillator (VCO) and Arbitrary Waveform Generator (AWG) before passing through an Electro-Optic Phase Modulator (EOPM). These components prior to the EOPM were necessary in the creation of Optical Frequency Combs, and were used in the feedback loop in lieu of the pump laser's installed Piezo.

4.1 Pound-Drever-Hall Technique Experiment

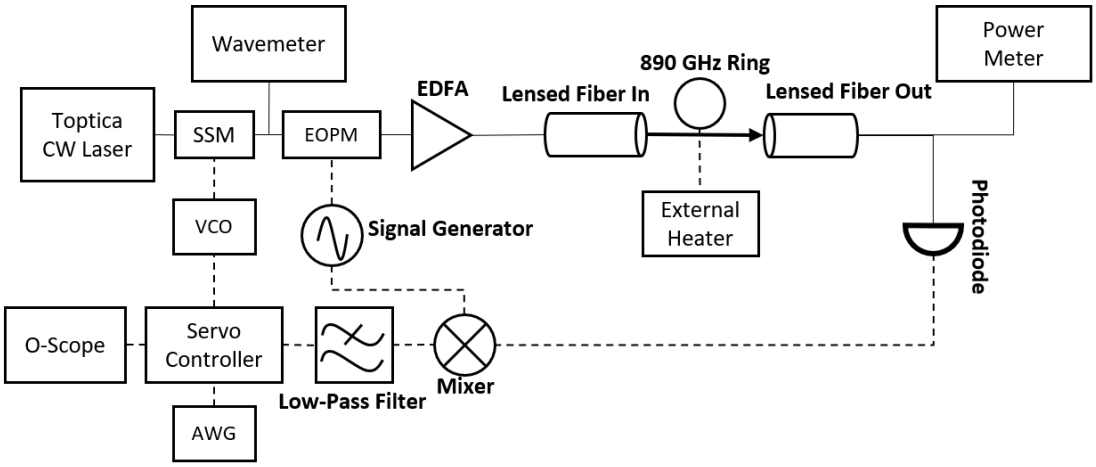

Figure 4.1. Experimental setup using a 890 GHz Free Spectral Range microring cavity

A Toptica CTL-1550 laser was used as the pump, and sent through a Single Sideband Modulator (SSM) controlled by a Voltage Controlled Oscillator (VCO). The SSM and VCO setup was the method used for pump frequency sweeping. The SSM and VCO setup were

used in lieu of the laser's PZT because they were necessary for the generation of optical frequency combs (OFC) using the microrings devices. Following the SSM, the pump light was split with one branch sent to a Menlo Systems Wavelength Meter WS/6-200 for wavelength measurement. Measurement of the pump light and power was needed to observe the transmission spectrum for when the pump was near resonance. The other branch was sent through a an EOSpace Lithium Niobate Electro-Optic Phase Modulator (EOPM) with a $V_{pi} = 3.0$@1GHz. The phase modulation was necessary in establishing the sidebands for the PDH technique. The phase modulated light then traveled through a Pritel Inc. Erbium-Doped Fiber Amplifier (EDFA) before using lensed fibers to couple to a microring with a rated FSR of 890 GHz with a Quality factor rated on the order of 5×10^6. The EDFA amplification was set to ensure a 4 mW output of the coupled ring setup. A Keithly 236 Source Measure Unit was connected to probes that contacted resistive pads installed on the microring chip to provide external heating. This heating was necessary to shift the resonance of the coupled microring, as well as generated comb frequency properties[27]. The ring output was split between a Thorlabs PM100A power meter, and a Lab Buddy Highly Linear Photodiode. The photodiode would then be able to generate an RF signal at the modulation frequency when the pump was close to resonance and amplified with a Lotus Systems Inc. LNA50M4G2S Amplifier with a rated gain of 36 dB. The RF signal was then mixed down to DC using a Mini-Circuits ZEM-4300 mixer along with a BLP-100+ Low-Pass Filter with 3-dB corner at 108 MHz. The signal generator used in phase modulation and mixing was an HP 8648C. An LB1005 Servo Controller (servo) took the mixed DC signal and repeated it to a Rohde & Schwarz RTO 1024 with 2 GHz bandwidth.

The servo used a sweep function generated by a Keysight 33600A Waveform Generator (AWG) output to the VCO for sweeping and pump control. This was performed by having the AWG output a 0 V to 1.4 V ramp function into the servo. The servo then passed this generated function on to the VCO, which can be seen in Figure 4.2. The VCO was set to output a 10 GHz signal to the SSM at a 0 V input. This meant that the pump light coupled into the microring was 10 GHz blue offset from the Toptica laser output. When the VCO received an input of 1.4 V, we calculated based on its specifications that its output

was approximately 12 GHz blue offset. This gave us a 2 GHz pump sweep range over the resonator as the servo swept the VCO input.

First, the setup described was used to prepare a lock of the pump to the microring. The VCO was swept using a 1.4 V_{pp} ramp function at 4 kHz, corresponding to ≈2 GHz sweep of the pump using the SSM. The signal generator was set to 199 MHz with an output of 10 dBm. Splitting its output, this meant that about 7 dBm reached the EOPM. This resulted in a detectable error signal, seen in Figure 4.2.

The sweep was then reduced and the servo was offset to output a V_{center} corresponding to 0 V input of the Error Signal, in this case $V_{center} \approx 0.5$ V. The PI lock was then engaged, and the servo reported a stable lock at settings $f_{PI} = 3$kHz, $K = 4.1$, and $s = 4$kHz, referencing equations 2.1 and 2.2. To test stability of the lock, we shifted the current of the external heater in order to shift the resonance of the microring, while monitoring the pump wavelength with the wavemeter. Fifteen measurements of the heater current and wavelength were taken, and the corresponding pump frequency shift was calculated between data points. The result of this data can be seen in Figure 4.3.

The lock appeared to track the resonance shifts for 1.8 GHz before the servo reported a failed lock. In this state, the pump was no longer frequency shifting with the heater due to voltage threshold settings on the servo to protect other equipment in the setup. The VCO setup could only accept a voltage range from 0 V to 4 V for safe operation, and we did not feel it was necessary to approach this voltage limit when we had a sufficient sweep range to perform a PDH lock. Further experimentation could be done by increasing the sweeping voltage from the servo to include the entire 0 V to 4 V range, which would have the expectation that the servo would be able to track any microring resonance shift applied by the external heater for a greater Δf frequency range.

To verify a lock had taken place, we then observed the resonance shifts in the transmission spectrum of the microring by utilizing the external heater again. With the VCO and signal generator off, the pump remotely swept over its Piezo (PZT) range near resonance. This process was repeated six more times with heater current starting at 63.0 and ending at 60.7 mA delivered to the microring resistive pads. During the PZT sweep, the wavemeter and power meter recorded the wavelength and power, with the data seen in Figure 4.4.

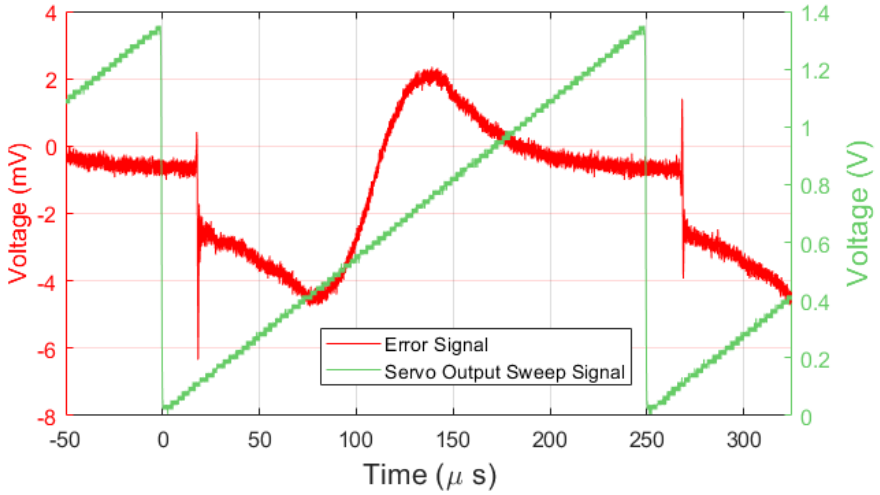

Figure 4.2. Observed error signal of 890 GHz Free Spectral Range microring using the Pound-Drever-Hall technique

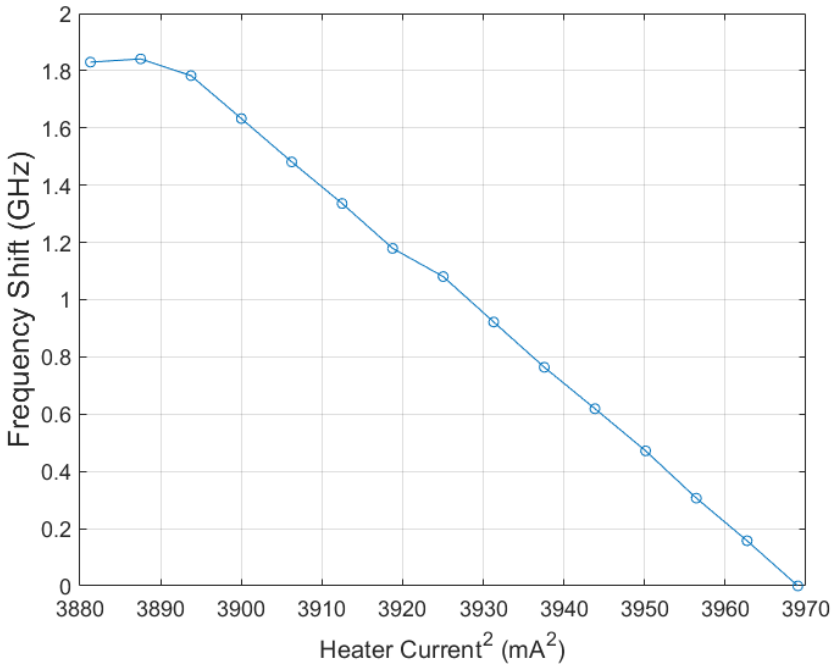

Figure 4.3. Observed pump frequency shift vs. heater settings with an engaged lock

Using this data, the wavelengths of the plotted minimums were taken as resonance (noted by the red circles in Figure 4.4) and used to correlate heater power for each trace vs. the frequency shift seen by the wavemeter. This is displayed in Figure 4.5 and shows a fairly

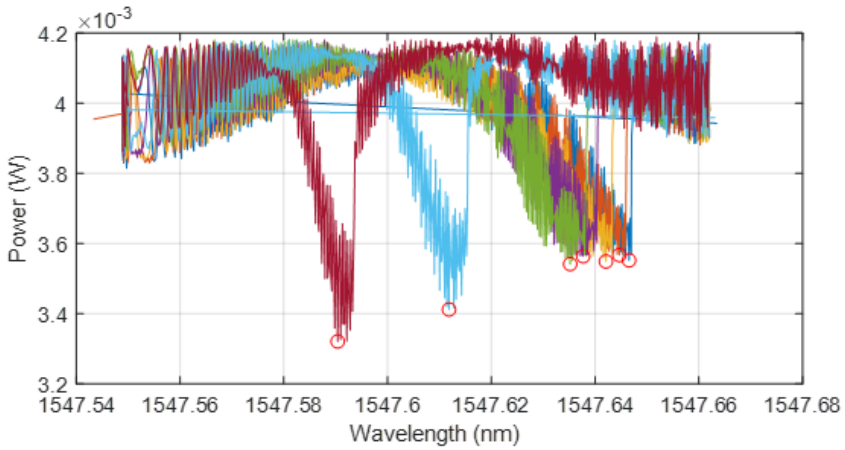

Figure 4.4. 890 GHz microring resonances with heater shifts applied

linear response in ring resonance to the square of supplied heater current. The square of the heater current was used because it was the controlled variable and the resistance of the installed ring pads were unknown. As a result, the power delivered to resistive pads on the ring would be proportional to the square of the heater current.

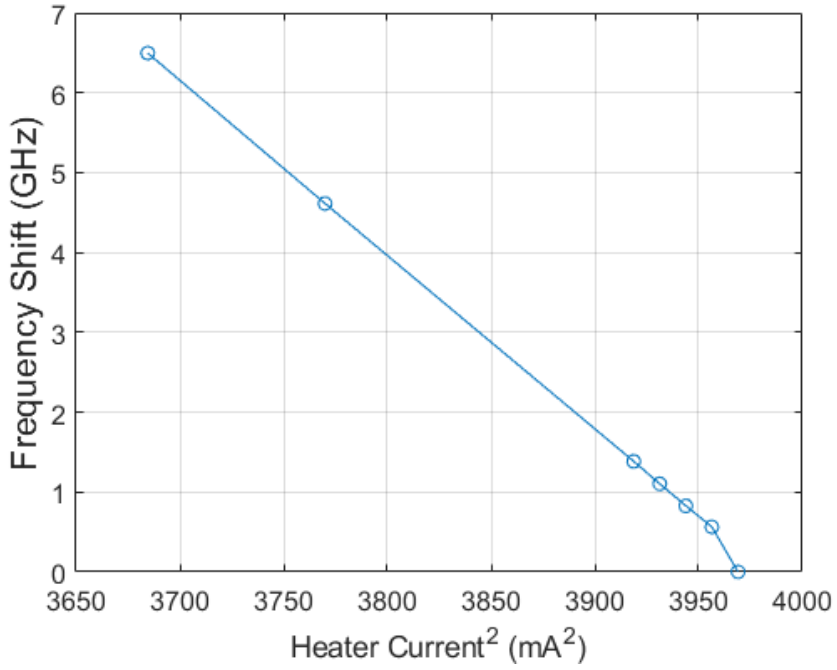

Figure 4.5. 890 GHz microring resonance Δf vs. heater power

With this data, we were able to correlate the Δf of the microring resonance when the pump was unlocked to the Δf of the pump when it was locked to the microring. The two previous plots (Figure 4.4 and Figure 4.5) were then plotted together and are shown in Figure 4.6. It is easy to see that both the resonance and locked pump shift at similar rates when the heater current is changed. This provided evidence that a PDH lock had been accomplished.

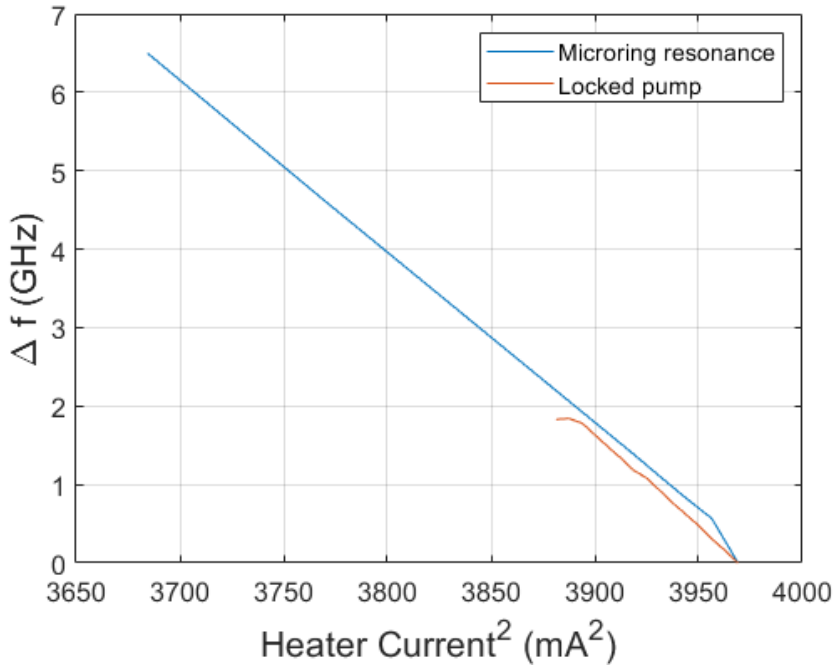

Figure 4.6. Δf of the locked pump and ring resonances vs. applied heater power

The next step in the experiment was to establish an OFC with the intention of generating a PDH lock afterwards. In Kerr soliton generation, the pump needs to be detuned from resonance in order to maintain an OFC. This requires an error signal with a zero-crossing point at the same frequency of the detuning in order for the PDH technique to be applied [28]. This can be done by phase modulating at the same frequency of the detuning.

In order to determine the correct modulation frequency, alterations to the setup were made, shown in Figure 4.7. An Agilent N5230C Vector Network Analyzer (VNA) output was applied to the phase modulator with the input after the RF amplifier. A coarse wavelength division multiplexer (CWDM) was installed at the output of the coupled microring. The CWDM was used to separate the pump and frequency comb power after the OFC was

generated. The pump light (≈1548 nm) would be separated and sent to the photodiode, while the light made of the modes that formed the frequency comb would be sent to an Optical Spectrum Analyzer. Any RF signal the photodiode output would be amplified and returned to the VNA.

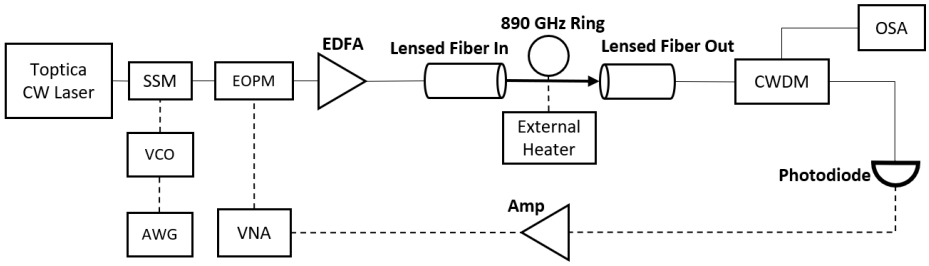

Figure 4.7. Detuning measurement with generated frequency comb

An OFC was then generated in the microring, such as the one shown in Figure 4.8, and a S_{21} trace was taken using the VNA. The type of OFC we were generating was a Dispersive Kerr Soliton (DKS) from the material properties of the microring. This was important because the pump center frequency is required to be offset while the DKS is active [18]. By measuring the S_{21} of the VNA, we intended to find the pump offset while a DKS was active in our 890 GHz microring.

The VNA swept from 300 kHz to 10 GHz, measuring the forward gain at each frequency. When a generated sideband crossed over the resonance of the microring, the photodiode would output an RF signal at the modulated frequency. Using the peak S_{21} from the VNA, it showed the pump appeared to be approximately 2.3 GHz away from resonance while the OFC was active, as shown in Figure 4.9.

In order to maintain the OFC, the pump's center frequency in relation to the microring resonance was considered fixed. This meant that any PDH technique conducted on the OFC generating ring was not going to lock the pump frequency to resonance. However, it is entirely possible to lock to an offset using a generated error signal, by locking to the sideband zero crossings[20] created in the resultant high-modulation error signal (as seen in Figure 1.4). This would create a frequency-stabilized pump that would not only be offset in frequency to the resonance by the modulation frequency used for the PDH technique, but

also allow a small range of tunability while the lock was active (this would be controlled by changing or sweeping the modulation frequency) [29]. Based on the results of the VNA S_{21} in Figure 4.9, we believed a phase modulation of ≈2.3 GHz should be sufficient to apply the PDH technique and lock the pump to the microring.

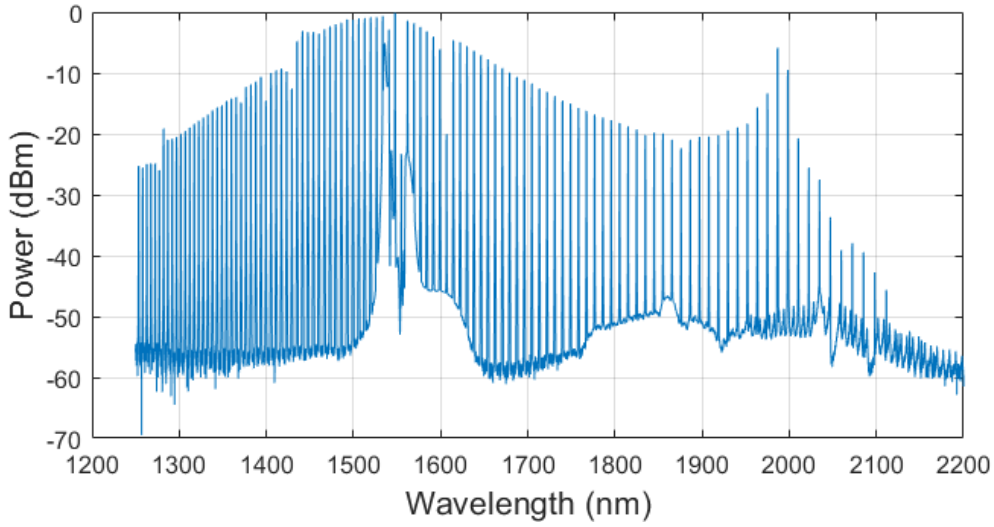

Figure 4.8. Optical Frequency Comb generated by 890 GHz Free Spectral Range microring

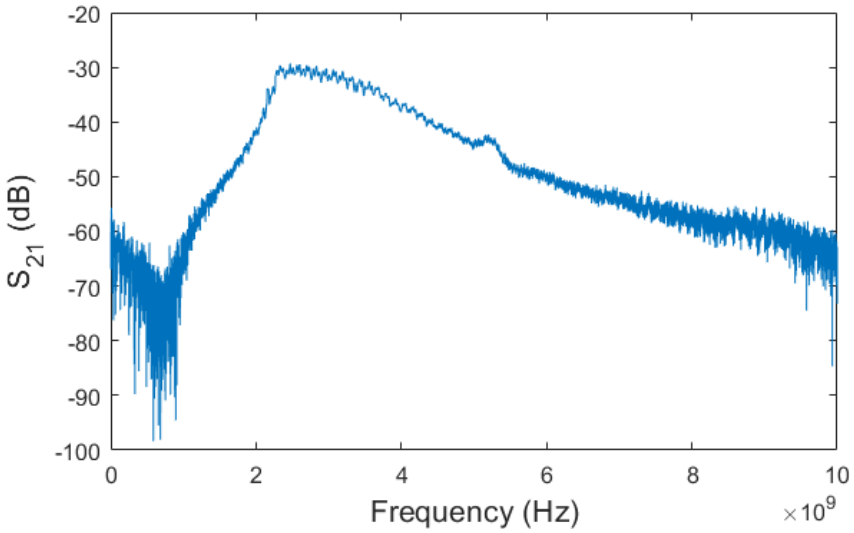

Figure 4.9. Vector Network Analyzer S_{21} while Optical Frequency Comb is generated from a microring

This process appeared straightforward, but was complicated by ensuring the shape of the error signal. As discussed previously from reference [10], a delay line or phase shifter is necessary to preserve the error signal amplitude when the frequency of modulation on the pump light becomes a set value. In the previous two experiments, this was not necessary because of the freedom in choosing the modulation frequency that would contribute to the error signal. In other words, the modulation frequency could be changed to ensure the minimum phase difference in the mixer inputs resulting in a maximum amplitude error signal. This was also not needed for Vector Network Analyzer (VNA) measurements in both the second and third experiment because the RF signal being input into the VNA in both cases had not been mixed with another RF signal, and no amplitude had been lost as a result of any mixing.

As the VNA was taking a S_{21} between its input and output, it was also used to measure the phase relationship between its two ports. Using this function, a phase delay measurement was taken for two paths. The first path measured was from the VNA through the microring and photodiode before returning to the VNA. The second measurement was taken for only the cable used in the PDH technique between the signal generator and the mixer (see Figure 4.1). The phase delay found can be seen in Table 4.1.

Table 4.1. Phase Delay Measurements of Signal Generator path in Figure 4.1

Path	Phase Delay
Through Resonator	$4.74 \times 10^{-}5\frac{^\circ}{Hz}$
Straight from Signal Generator to Mixer	$2.09 \times 10^{-}5\frac{^\circ}{Hz}$

With this data, it was calculated that a phase delay line of 13.2 meters was needed to ensure phase matching prior to mixing. This length would be expected to generate a loss of 4.5 dB using exclusively SMA connections at 2.3 GHz, and 14 dB loss using the BNC cable on hand. Without the requisite lengths of SMA cable on hand to keep loss at an acceptable level, utilizing the PDH technique on a microring generating an OFC was paused to pursue other OFC experimentation.

4.2 Optical Clock Implications

Utilizing similar high repetition rate microrings, an application to generate and beat together two OFCs has been experimented with to generate a beat between two comb lines. In the case where two high FSR microrings are used, there exists a pair of comb lines where the N-th comb line of the higher rep-rate comb catches the $N+1$-th comb line of the lower rep-rate comb. If the difference of the repetition rates of the rings can be detected, then mixing the first pair of comb lines along with the N_{high}-th and $N_{low}+1$-th pair will generate a N-th division of f_{rep} [30] [31]. This is known as Vernier frequency division. Applying this to an optical clock, the detection and locking of the Vernier beat generated would be the necessary step in generating a detectable microwave signal for the clock system. This, in addition to locking the f_{CEO} would make a microring optical clock system viable.

5. CONCLUSION

In summary, the research and experiments presented here demonstrated the application and use for the Pound-Drever-Hall technique, as well as future application it may have in compact optical clock systems. The capability to use PDH on silicon nitride optical microrings in conjunction with OFC generation may be a necessary tool in obtaining a stable optical system.

In the future, further experimentation may be explored in regards to both scope and application. All of the PDH techniques performed in the described experiments were measured and confirmed over a short time scale, on the order of an hour. Were the experiments to be repeated, longer time scales of the locks could be explored to asses the drift between a pump and resonant cavity over days or weeks. This may require the use of an additional coarse-control locking mechanism that could counter the long term drift, perhaps in the form of pump or cavity temperature control. Other factors such as improvement of DC noise could be implemented [12]. This may be accomplished through using more RF blocking at the output of a mixer to better isolate the DC component, as well as using a phase-shifter or delay line to minimize the phase difference in the mixer's inputs. Additionally, application of the PDH technique to a microring cavity generating an Optical Frequency Comb would be a logical continuation [28] [29] [20], requiring a PDH technique to be accomplished with a set offset frequency between cavity resonance frequency and the pump's frequency.

Regardless of laser locking methods, the power of low power, miniature OFC sources may have a large impact on the future of timekeeping systems. GNSS, inertial navigation systems used by aircraft and large ships, and even complex encryption methods often rely on local and accurate timekeeping. Optical systems that improve upon these timekeeping methods will only enhance the reliability and certainty of complex infrastructures in use today.

REFERENCES

[1] G. E. Marti, R. B. Hutson, A. Goban, S. L. Campbell, N. Poli, and J. Ye, "Imaging optical frequencies with 100 μ hz precision and 1.1 μ m resolution," *Physical review letters*, vol. 120, no. 10, p. 103 201, 2018.

[2] M. Takamoto, I. Ushijima, N. Ohmae, T. Yahagi, K. Kokado, H. Shinkai, and H. Katori, "Test of general relativity by a pair of transportable optical lattice clocks," *Nature Photonics*, vol. 14, no. 7, pp. 411–415, 2020.

[3] T. Fortier and E. Baumann, "20 years of developments in optical frequency comb technology and applications," *Communications Physics*, vol. 2, no. 1, pp. 1–16, 2019.

[4] T. Schuldt, M. Gohlke, M. Oswald, J. Wüst, T. Blomberg, K. Döringshoff, A. Bawamia, A. Wicht, M. Lezius, K. Voss, *et al.*, "Optical clock technologies for global navigation satellite systems," *GPS Solutions*, vol. 25, no. 3, pp. 1–11, 2021.

[5] A. K. Ghatak, *Optical electronics*. Cambridge England New York: Cambridge University Press, 1989, p. 254, ISBN: 0-521-30643-4.

[6] R. Drever, J. L. Hall, F. Kowalski, J. Hough, G. Ford, A. Munley, and H. Ward, "Laser phase and frequency stabilization using an optical resonator," *Applied Physics B*, vol. 31, no. 2, pp. 97–105, 1983.

[7] R. V. Pound, "Electronic frequency stabilization of microwave oscillators," *Review of Scientific Instruments*, vol. 17, no. 11, pp. 490–505, 1946.

[8] E. S. Magden, M. Y. Peng, J. D. Bradley, G. Leake, D. D. Coolbaugh, L. A. Kolodziejski, F. X. Kärtner, and M. R. Watts, "Laser frequency stabilization using pound-drever-hall technique with an integrated tio2 athermal resonator," in *CLEO: Science and Innovations*, Optical Society of America, 2016, STu1H–3.

[9] C. Fabry, "Theorie et applications d'une nouvelle methods de spectroscopie intereferentielle," *Ann. Chim. Ser. 7*, vol. 16, pp. 115–144, 1899.

[10] E. D. Black, "An introduction to pound–drever–hall laser frequency stabilization," *American journal of physics*, vol. 69, no. 1, pp. 79–87, 2001.

[11] M. Suter and P. Dietiker, "Calculation of the finesse of an ideal fabry–perot resonator," *Applied optics*, vol. 53, no. 30, pp. 7004–7010, 2014.

[12] G. C. Bjorklund, M. Levenson, W. Lenth, and C. Ortiz, "Frequency modulation (fm) spectroscopy," *Applied Physics B*, vol. 32, no. 3, pp. 145–152, 1983.

[13] T. Udem, R. Holzwarth, and T. W. Hänsch, "Optical frequency metrology," *Nature*, vol. 416, no. 6877, pp. 233–237, 2002.

[14] P. Del'Haye, O. Arcizet, A. Schliesser, R. Holzwarth, and T. J. Kippenberg, "Full stabilization of a microresonator-based optical frequency comb," *Physical Review Letters*, vol. 101, no. 5, p. 053 903, 2008.

[15] F. Riehle, *Frequency standards: basics and applications*. John Wiley & Sons, 2006.

[16] P. Del'Haye, A. Schliesser, O. Arcizet, T. Wilken, R. Holzwarth, and T. J. Kippenberg, "Optical frequency comb generation from a monolithic microresonator," *Nature*, vol. 450, no. 7173, pp. 1214–1217, 2007.

[17] X. Xue, Y. Xuan, Y. Liu, P.-H. Wang, S. Chen, J. Wang, D. E. Leaird, M. Qi, and A. M. Weiner, "Mode-locked dark pulse kerr combs in normal-dispersion microresonators," *Nature Photonics*, vol. 9, no. 9, pp. 594–600, 2015.

[18] T. J. Kippenberg, A. L. Gaeta, M. Lipson, and M. L. Gorodetsky, "Dissipative kerr solitons in optical microresonators," *Science*, vol. 361, no. 6402, eaan8083, 2018.

[19] A. Abramovici, W. E. Althouse, R. W. Drever, Y. Gürsel, S. Kawamura, F. J. Raab, D. Shoemaker, L. Sievers, R. E. Spero, K. S. Thorne, *et al.*, "Ligo: The laser interferometer gravitational-wave observatory," *science*, vol. 256, no. 5055, pp. 325–333, 1992.

[20] Z. L. Newman, V. Maurice, T. Drake, J. R. Stone, T. C. Briles, D. T. Spencer, C. Fredrick, Q. Li, D. Westly, B. R. Ilic, *et al.*, "Architecture for the photonic integration of an optical atomic clock," *Optica*, vol. 6, no. 5, pp. 680–685, 2019.

[21] A. Jeanmaire, P. Rochat, and F. Emma, "Rubidium atomic clock for galileo," in *Proceedings of the 31th annual precise time and time interval systems and applications meeting*, 1999, pp. 627–636.

[22] R. Sabatini, L. Aulanier, G. Marinoni, M. Martinez, B. Pour, and H. Rutz, "Multifunctional information distribution system (mids) low volume terminal (lvt) development and integration programs towards link-16 network centric allied/coalition operations," *NATO: OTAN, MIDS International Program Office*, 2007.

[23] J. Nilsson and H. Lans, "A gnss-based time division multiple access data link," *Air Traffic Control Quarterly*, vol. 1, no. 4, pp. 353–363, 1993.

[24] X. Zhu, M. You, Y. Shi, B. Yang, and J. Liu, "Pound-drever-hall locking system for precise temperature measurement based on silicon ring resonators," in *2022 IEEE 35th International Conference on Micro Electro Mechanical Systems Conference (MEMS)*, IEEE, 2022, pp. 130–133.

[25] D.-S. Seo, C. Park, D. E. Leaird, and A. M. Weiner, "Improvement of a pound-drever-hall technique to measure precisely the free spectral range of a fabry-perot etalon," *Journal of the Optical Society of Korea*, vol. 19, no. 4, pp. 357–362, 2015.

[26] D. E. Leaird, A. M. Weiner, and D. Seo, "Wideband flat optical frequency comb generated from a semiconductor based 10 ghz mode-locked laser with intra-cavity fabry-perot etalon," *Journal of IKEEE*, vol. 18, no. 1, pp. 19–24, 2014.

[27] X. Xue, Y. Xuan, C. Wang, P.-H. Wang, Y. Liu, B. Niu, D. E. Leaird, M. Qi, and A. M. Weiner, "Thermal tuning of kerr frequency combs in silicon nitride microring resonators," *Optics express*, vol. 24, no. 1, pp. 687–698, 2016.

[28] J. R. Stone, T. C. Briles, T. E. Drake, D. T. Spencer, D. R. Carlson, S. A. Diddams, and S. B. Papp, "Thermal and nonlinear dissipative-soliton dynamics in kerr-microresonator frequency combs," *Physical review letters*, vol. 121, no. 6, p. 063 902, 2018.

[29] E. G. A. Lucas, "Physics of dissipative kerr solitons in optical microresonators and application to frequency synthesis," EPFL, Tech. Rep., 2019.

[30] M. S. Alshaykh, C. Wang, N. P. O'Malley, Z. Ye, A. Al Noman, D. E. Leaird, M. Qi, A. M. Weiner, *et al.*, "Optical dual-comb vernier division of an octave-spanning kerr microcomb," in *CLEO: Science and Innovations*, Optica Publishing Group, 2021, SW2H–7.

[31] B. Wang, Z. Yang, X. Zhang, and X. Yi, "Vernier frequency division with dual-microresonator solitons," *Nature communications*, vol. 11, no. 1, pp. 1–7, 2020.